ความสัมพันธ์ระหว่างความสามารถในการไหลและโครงสร้างจุลภาคของโลหะผสมอะลูมิเนียม ซิลิกอน

นาย ทราน ดุก ฮุย

วิทยานิพนธ์นี้เป็นส่วนหนึ่งของการศึกษาตามหลักสูตรปริญญาวิศวกรรมศาสตรมหาบัณฑิต
สาขาวิชา วิศวกรรมโลหการ ภาควิชาวิศวกรรมโลหการ
คณะวิศวกรรมศาสตร์ จุฬาลงกรณ์มหาวิทยาลัย
ปีการศึกษา 2546

SBN 974-17-4815-9

RELATIONSHIP BETWEEN FLUIDITY AND MICROSTRUCTURE OF ALUMINUM SILICON ALLOY

Mr. Tran Duc Huy

A Thesis Submitted in Partial Fulfillment of the Requirements
for the Degree of Master of Engineering in Metallurgical Engineering
Department of Metallurgical Engineering
Faculty of Engineering
Chulalongkorn University
Academic Year 2003

ISBN 974-17-4815-9

Thesis Title : Relationship between Fluidity and Microstructure of Auminum-Silicon Alloy

By : Mr. Tran Duc Huy
Field of Study : Metallurgical Engineering
Thesis Advisor : Assistant Professor Ittipon Diewwanit, Sc.D.
Thesis Co-advisor : Professor Umeda Takateru, D.Eng.

Accepted by the Faculty of Engineering, Chulalongkorn University, in partial fulfillment of the requirements for the Degree of Master of Engineering.

..... Dean of the Faculty of Engineering
(Professor Direk Lavansiri, Ph.D.)

Thesis Committee:

..... Chairman
(Associate Professor Prasonk Sricharoenchai, D.Eng.)

..... Thesis Advisor
(Assistant Professor Ittipon Diewwanit, Sc.D.)

..... Thesis Co-advisor
(Professor Umeda Takateru, D.Eng.)

..... Member
(Suvanchai Pongsugitwat, M.Eng.)

ทราน ดุก ฮุย : ความสัมพันธ์ระหว่างความสามารถในการไหลและโครงสร้างจุลภาคของโลหะผสมอะลูมิเนียมซิลิคอน. (RELATIONSHIP BETWEEN FLUIDITY AND MICROSTRUCTURE OF ALUMINUM ALLOY) อ.ที่ปรึกษา: ผู้ช่วยศาสตราจารย์ ดร. อิทธิพล เดี่ยววนิชย์, อ.ที่ปรึกษาร่วม: Professor Umeda Takateru; 80 หน้า. ISBN 974-17-48159

ความสามารถในการไหลของโลหะผสมหล่อสามารถนิยามได้ว่าคือ ความสามารถของน้ำโลหะหลอมเหลวที่ไหลเข้าไปเติมเต็มช่องว่างในแบบหล่อได้อย่างสมบูรณ์ ในการศึกษานี้ได้ทำการตรวจวัดความสามารถในการไหลของโลหะอะลูมิเนียมผสมประกอบด้วยเกรด AC2B, AC4CH, AC4B, AC9A, ADC12 และ ADC14 ด้วยวิธีดูดน้ำโลหะเข้าท่อภายใต้ความดันลด ตัวแปรต่างๆ ที่ควบคุมในการศึกษานี้ได้แก่ ชนิดวัสดุที่ใช้ทำท่อ (เหล็กกล้าไร้สนอม ทองแดง และ ควอทซ์) เส้นผ่านศูนย์กลางภายในของท่อ (ระหว่าง 2-6 มิลลิเมตร) ความดันต่างที่ใช้ดูดน้ำโลหะ (ระหว่าง 1.33 – 95 กิโลปาสกาล) และระดับของการให้ความร้อนเหนือจุดหลอมเหลว (ระหว่าง 0 – 120 เคลวิน) ผลการทดลองแสดงให้เห็นว่า ความสามารถในการไหลของโลหะอะลูมิเนียมทุกเกรดแปรผันตรงกับรากที่สองของความดันที่ใช้สำหรับดูดน้ำโลหะ (applied suction pressure) ในทุกสภาวะการทดลอง ความสามารถในการไหลของโลหะผสมอะลูมิเนียมซิลิคอนที่มีปริมาณซิลิคอนมากกว่า จะมีความสามารถในการไหลสูงขึ้น และเมื่อนิยามค่าความดันประสิทธิผล (effective suction pressure) จากผลต่างของความดันที่ใช้ดูดน้ำโลหะ กับพจน์ของความดันต้านอันเนื่องจากแรงโน้มถ่วงและพลังงานพื้นผิว ความดันประสิทธิผลจะแปรผันตรงกับความสามารถในการไหล ในทางทฤษฎีสามารถคำนวณพลังงานพื้นผิวได้จากผลการทดลองนี้ โดยใช้สมการถดถอยเชิงเส้นที่ผ่านจุดกำเนิดค่าความดันที่น้อยที่สุดที่สามารถดูดน้ำโลหะอะลูมิเนียมผสมมีค่าอยู่ระหว่าง 40 ถึง 200 ปาสกาล โครงสร้างจุลภาคของชิ้นงานทดสอบที่แข็งตัวแล้วเป็นไปตามทฤษฎีและกลไกการไหลของน้ำโลหะผ่านช่องของเหลวแคบ ดังที่เสนอก่อนหน้านี้โดย Flemings

ภาควิชา .....วิศวกรรมโลหการ.....ลายมือชื่อนิสิต.....
สาขาวิชา.....วิศวกรรมโลหการ.....ลายมือชื่ออาจารย์ที่ปรึกษา.....
ปีการศึกษา.....2546.....ลายมือชื่ออาจารย์ที่ปรึกษาร่วม.....

4570706521: MAJOR METALLURGICAL ENGINEERING
KEYWORD: SOLIDIFICATION, FLUIDITY, ALUMINUM ALLOYS SUCTION PRESSURE

TRAN DUC HUY: FLUIDITY TEST OF ALUMINUM ALLOYS INTO A VACUUM MOLD. THESIS ADVISOR: ASSITANCE PROFESSOR ITTIPON DIEWWANIT, THESIS CO-ADVISOR: PROFESSOR UMEDA TAKATERU, 80 pp. ISBN 974-17-48159

Fluidity of casting alloys is defined as the ability of molten metal to fill mold cavity completely. In this research, fluidity of aluminum alloy grade AC2B, AC4CH, AC4B, AC9A, ADC12, and ADC14 was measured using reducing vacuum technique. Other parameters such as tube materials (copper, stainless steel, and quartz), tube diameters (from 2 mm to 6 mm), applied suction pressure (from 1.33 to 95 kPa), and degree of superheat (from 0 to 120 K) are investigated. Fluidity length of every alloy and condition varies linearly with the square root of suction pressure. Alloys with high silicon content exhibit higher fluidity. Effective suction pressure, defined as applied suction pressure minus gravity and surface energy terms, varies linearly with fluidity. Theoretical analysis indicates that the surface energy can be calculated from the experiments by fitting with curves which pass through the origin. Minimum applied suction pressure required to suck the liquid was calculated and is in the range from 40 to 200 Pa depending on the type of alloys. Microstructure of solidified specimen in the tubes was observed and agrees with the fine channel flow mechanism proposed earlier by Flemings.

Department…Metallurgical Engineering…Student signature……..
Field of study..Metallurgical Engineering.Advisor's signature……
Academic year…….2003……..Co-advisor's signature……...

ACKNOWLEDGEMENTS

With the help and support from various organizations and people, I could complete my study. Thus, I would like to express my appreciation and grateful thanks to:

The JICA Project for AUN/SEED-Net (ASEAN University Network / Southeast Asia Engineering Education Development Net Work) for providing me the scholarship to study at Chulalongkorn University.

The International School of Engineering (ISE), Chulalongkorn University for giving me the chance to have the scholarship to study at Chulalongkorn University.

I would like to express my deep gratitude to my advisors: Asst Prof Ittipon Diewwanit and Professor Umeda Takateru for their teachings, helps and recommendations.

Also, I would like to send my great gratitude to all professors of the Department of Metallurgical Engineering, Faculty of Engineering, Chulalongkorn University, for their guides and helps during the time I have studied in Chulalongkorn University. My special thanks to Assist. Prof Charkorn Jarupisitthorn, Aj. Suvanchai Pongsukitwat and Aj. Patama Visuttipitukul for their valuable comments and academic suggestions on my research work.

My appreciation goes to my friends for their enthusiasm and all what they have done for me during my study in Thailand.

Last but not least, my special thanks go to all members of my family for what they have done for me when I have studied far from home. Without their help I could not be able to complete my study.

CONTENTS

CONTENTS (continued)

List of Tables

Table **Page**

List of Figures

List of Figures (continued)

List of Figures (continued)

List of Figures (continued)

Chapter 1

Introduction

1.1 Back ground

Metal casting is reported to be a prehistoric event that appears, on the archeological record, after evidence of earlier metalworking. It is assumed that the earliest castings were made from native metals and alloys at least 10,000 years ago. Among the first metal to be cast by humankind are copper, iron, gold, silver, etc. whereas aluminum is one of the newest. Aluminum casting became affordable only after the invention of aluminum refining by the Hall-Heroult process. In the early part of the 20^{th} Century, the application of aluminum casting was limited to decorative parts and cooking utensils. After World War II, a dramatic expansion of aluminum casting industry occurred. And now, aluminum is the most heavily consumed non-ferrous metal in the world, with current annual consumption at 24 million ton. This can be understood with the main advantages of aluminum is light weight and good castability; therefore saving materials and energy. While the opportunities are growing, aluminum must continue to be completed with various materials that offer lower cost or other competitive advantages.

A wide range of metals can be added to aluminum. Among those regularly added and controlled as alloying elements are zinc, magnesium, copper, silicon, iron, lithium, manganese, nickel, silver, tin and titanium. Some of them will prove their properties allowing, in some cases, for heat treating, but others will be detrimental.

Fluidity of casting alloys is defined as the ability of molten metal to completely fill a mold cavity. It is of significant effect in producing sound thin wall casting. Fluidity has been measured in several ways but the two most commonly adopted are spiral and vacuum fluidity test. In these test, liquid metal flows in a long tube until flow is stopped by solidification. Fluidity is measured quantitatively as the length of the metal flows before it is stopped. Fluidity spiral test mostly is used in factory, and the vacuum fluidity test is used in laboratory.

In studying the characteristic of fluidity, it is necessary to understand the relationship between fluidity and structure; therefore, we can predict, and controlled property of alloy. Aluminum alloys are widely used, especially in automobile and aviation industry due to the need for light-weight parts. It is used in many machinery parts: wheel – casting, cylindrical and block engine.

Nowadays, die-casting is gradually popular, and almost is operated with aluminum alloys to produce machinery parts. In die-casting, always cast with the very thin wall mold, so understanding of fluidity of aluminum alloys is required to avoid some misruns caused by fluidity property.

Although there are a lot understandings about the heat transfer during solidification and microstructure of aluminum alloys system, the relationships among these and rheological properties of the fluid are still interested. This study aims at the relations between the structure of the fluid and its internal structure with implications for permanent mold casting, die-casting to reduce defects and improve quality for the processes.

1.2 Objectives of research

The objectives of this research are:

- To determine the fluidity of aluminum alloys
- To determine the effect of degree of superheat to fluidity
- To determine relationship between fluidity and microstructure
- To clarify the criteria of the flow cessation

Chapter 2

Literature survey

2.1 Solidification of aluminum alloys

It is not very common to produce cast pieces from pure aluminum since they are soft and their properties are poor. However, adding of other elements, especially silicon will increases fluidity - the filling capacity and allows obtaining the intricate shapes. Solidification proceeds through a series of mechanisms, which can be used to control the properties of the casting.

2.1.1 Nucleation and growth

Transition from the liquid to solid occurs by nucleation and growth in classical theory of nucleation, the radius of a spherical stable embryo (r^*) is given by:

$$r^* = \frac{2\gamma_{sl}T_m}{L\Delta T}$$

where γ_{sl} is the solid-liquid interfacial free energy, L is the latent heat of transformation per unit volume, ΔT is the undercooling and T_m is the melting temperature. The critical energy of activation (ΔG^*) for an embryo of radius r^* is given by:

$$\Delta G^* = \frac{16}{3}\pi\frac{\gamma_{sl}T_m^2}{L^2\Delta T^2}$$

Homogeneous nucleation is only possible for high undercooling (on the order of $0.25T_m$). However, any surface, such as cavities, walls or solid

particles, may catalyze nucleation at a much smaller undercooling and with fewer atoms required to form the nucleus, following the phenomenon known as heterogeneous nucleation.

Once the nuclei are stable they will start to growth at a rate controlled by the atomic mobility across the solid-liquid interface, and by mass and heat transfer. Solidification implies that at a given time more atoms move from the liquid side of the interface to the solid one that in the other direction. Growth also implies that the interface keeps moving and increasing in size in such a way that solidification will only proceed if the temperature of the interface is below the melting temperature (T_m) due to the necessity to compensate the interfacial free energy (γ_{sl}) and the latent heat of solidification

2.1.2 Microstructure

A series of parameter can be employed to describe the metallurgical microstructure of aluminum casting. Separation between dendrite arms is affected by the solidification rate, distribution and aspect of the eutectic aggregate, as well as grain size, can be controlled by addition of elements or compounds and by cooling rate. Size and distribution of intermetallic phases is much more complex, since care has to be taken on impurities content and concentration as well as other solidification condition.

a. Dendrite arm spacing

Solidification of commercial alloys is proceeded by formation of dendrite from the liquid. This is especially the case in hypoeutectic aluminum-silicon alloys, in which the dendrites will be of primary

aluminum. Distance or separation between the different dendrite arms is normally measured on the secondary branches, rather than on the primary ones. For a given composition, it is controlled exclusively by the solidification rate. Microstructure examination can be used to obtain information related to the rate or time involved during solidification at different places within a complex cast by reference to data obtained in controlled unidirectional solidified trials.

Engineering castings can be improved by optimization of the dendrite arm spacing (DAS), since both mechanical and physical properties are enhanced when this parameter diminishes.

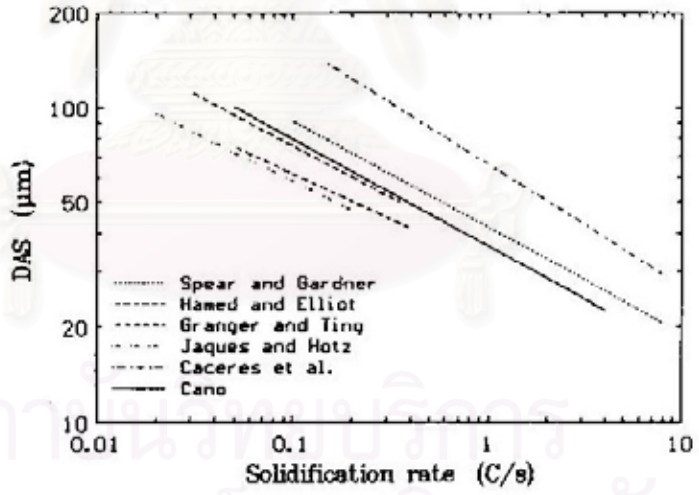

Figure 1. Secondary dendrite arm spacing (DAS) as a function of solidification rate [20]

b. Intermetallic

The most common intermetallic phases found in aluminum alloy are related to contamination with iron, which has limited solubility in liquid aluminum.

Of these intermetallic phases, ***β***- Al_5FeSi is the most detrimental to mechanical properties due to its needle shape microstructure (figure 2) and its low coherency with the aluminum matrix. Addition of manganese transform these intermetallic into the less deleterious ***α***- $Al_{15}(FE, Mn)_3Si_2$ phase which due to its aspect. Figure 2 is commonly referred to Chinese script. A drawback of addition of manganese is the increase in both hardness and quantity of intermetallic particles for a given iron content, in such way that the positive effect of manganese on the modification of the intermetallic morphology to increase the resistance to crack propagation is offset by the increase brittleness and volume of the ***α*** particles.

Intermetallic phases can be form in aluminum casting at high temperatures before the aluminum dendrites are formed, concurrently with the solidification of the alloy, or they can form complex eutectic phase which solidifies at temperatures as low as 480^0C. A short summary of the intermetallic phases encountered in aluminum- silicon alloy is presented in table 1.

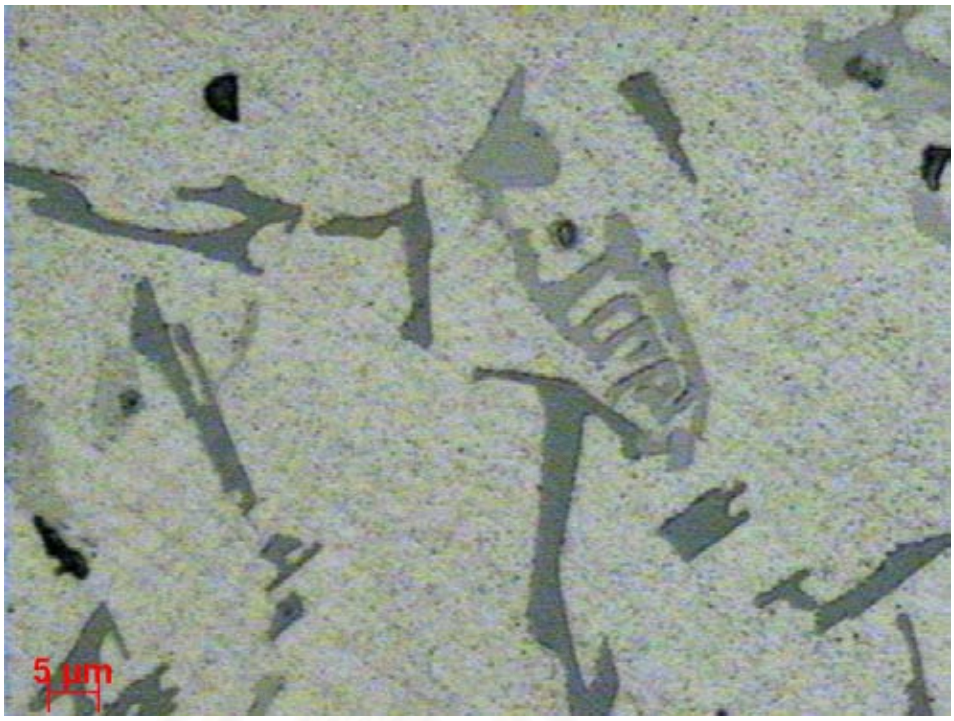

Figure 2. Microstructure of AC4CH at the inlet gate of the tube. Magnification 50x

Table 1. Intermetallic phases in aluminum- silicon alloys

Reaction	Phases
Pre- dendritic	$Al_{15}(Fe, Mn)_3Si_2$
Post- dendritic	$Al_{15}(Fe, Mn)_3Si_2$- Al_5FeSi
Eutectic	Al_5FeSi- Mg_2Si
Post- eutectic	$Al_5Mg_8Cu_2Si_6$- $CuAl_2$

Two factors which are known to control the morphology and nature of the intermetallic found in cast alloy are the solidification rate and the chemical composition. The solidification rate exerts a direct impact on the

kinetics and amount of iron rich phases present in the microstructure. Low cooling rate favors the formation of β needles which are formed in well defined crystallographic planes, whereas higher rate tends to favor the Chinese script type. Experimental results show that the transition between β and α takes place at slower rate as amount of iron is reduced. Several authors have shown that the element that controls the transition from β to α depend on the amount of Fe, Mn, Cr as the former increase β formation is promoted, while Mn and Cr contribute to the stabilization of α particles.

There are some ways to reduce the detrimental effect of iron intermetallic:

- Maintain low iron levels
- Maintain a Mn/Fe ratio higher than 0.5
- Increase solidification rate
- Reduce the degree of eutectic modification

2.2 Fluidity

In shape casting processes, metal enters the mold through one or a number of gates. Should it then fail to fill the cavity before it solidifies, it is said to be insufficiently fluid. Thus, the term “fluidity” has come to mean something quite different to the foundryman than to the physicist. To the physicist, it is the reciprocal of viscosity; to the foundryman, it is an empirical measure of a processing characteristic. The foundryman measures this property in one of several types of fluidity test. In these tests, hot metal is caused to flow in a long channel of a small cross section (channel is at room temperature). The length of the metal flows before it is stopped by

solidification is the measure of fluidity. Two common types are the fluidity spiral and the vacuum fluidity test which sketch below [1]:

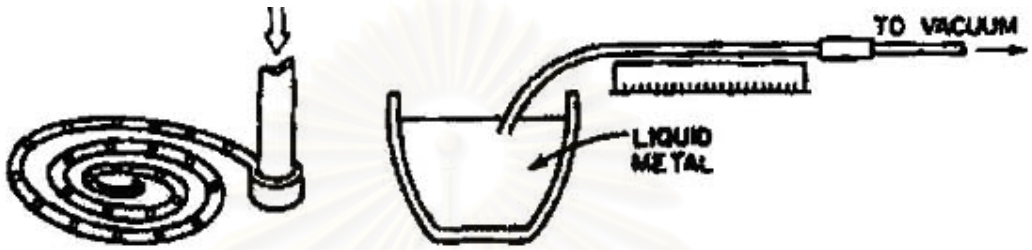

Figure 3. Fluidity tests

Fleming's solidification model shows the fluidity of pure metals and alloys pouring at its melting point in fluidity tests channel quite different. The instant this metal enters the channel, solidification begins at the channel entrance. As it proceeded down the channel, solidification begins in these locations also. However, because freezing began first at the channel entrance, it is here that the flow choked off. The total length the metal flow before stopping is the fluidity

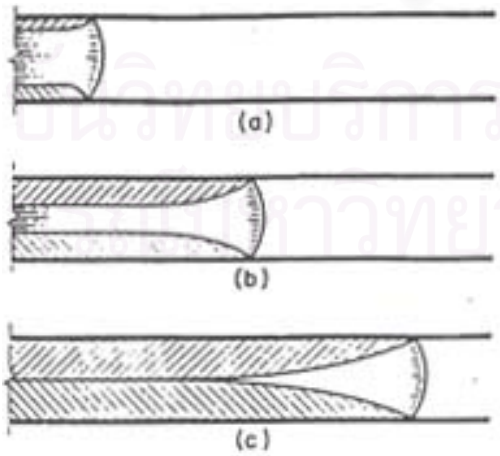

Figure 4. Flow and solidification of a pure metal in a fluidity channel [1].

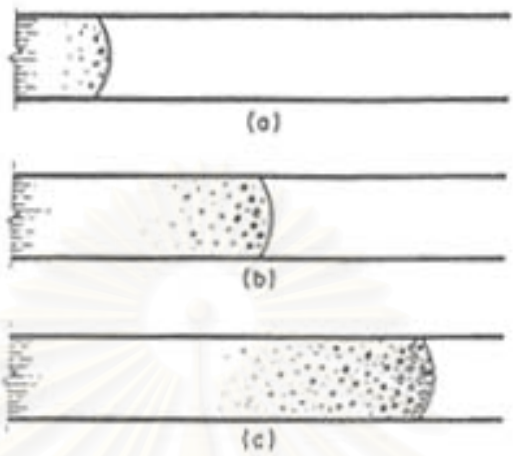

Figure 5. Flow and solidification of alloy in a fluidity channel [1].

In pure metals, when metal enters the channel of fluidity test, solidification begins at the channel wall and continues by growth of columnar grains with planar interface as metal flows through the channel. Flow ceases when the columnar grains abut each other at the channel entrance. But in alloys, flow ceases at the leading tip of the flowing stream where it form columnar dendrites. The dendrite arms are exposed and fracture forming equiaxed grains.

The above figure illustrates the foregoing process. Fluidity determined as above is influenced by:

- Metal variables such as temperature, viscosity, and heat of fusion.
- Mold and mold-metal variables such as heat-flow resistance at the interface, mold conductivity, density, and specific heat.
- Test variable such as applied metal head and channel diameter.

Solidification of AC4CH alloy

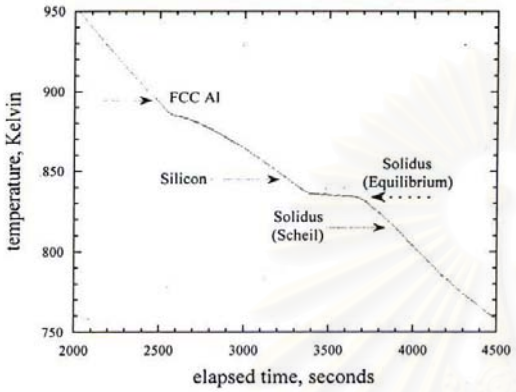

Figure 6. Cooling curve of AC4CH alloy

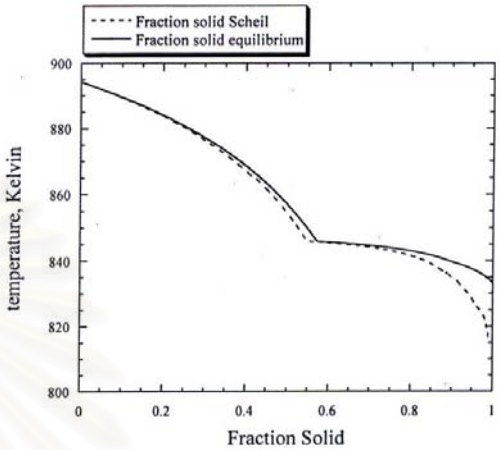

Figure 7. Fraction of solid vs. temperature of alloy AC4CH

Solidification of AC4CH aluminum alloy begins with the crystallization of primary aluminum fcc. This is followed by the nucleation of solid silicon subsequent precipitation of intermetallic phases are Al_5FeSi, $Al_8Mg_3FeSi_6$, Mg_2Si

Brief summary effect of some alloying elements:

* Copper is employed to increased strength and hardness in heat treatable alloys, this element exhibits detrimental effect like reduction in general corrosion resistance, to hot tearing and in castability.

* Magnesium contributes to increase in hardness and strength in aluminum-silicon alloy since Mg_2Si solubility is temperature dependent.

* Manganese is considered to be an impurity in casting and is controlled to a minimum level. It combines with iron to form insoluble phases.

* Iron improves hot tear resistance and reduce tendency for die sticking or soldering in die casting. Increment in iron content reduces, however, ductility and machinability. Iron forms a series of insoluble intermetallic compound which affect the properties of a casting.

* Nickel is used in combination with copper to enhance high temperature properties.

* Calcium is a weak eutectic modifier agent, but it is scarcely used due to the increase of hydrogen solubility which is often responsible for casting porosity

* Titanium is extensively used to refine grain size in aluminum castings. It is commonly employed in combination with boron

* Tin is effective in reducing friction and it is employed in bearing applications.

* Zinc is added to aluminum in some alloys due to the excellent response to age hardening.

* Silicon: The fluidity of aluminum-silicon alloys as a function of silicon content. At constant pouring temperature, the maximum fluidity was obtained at a composition of about 13-14%Si. However, fluidity is continuously increased beyond the eutectic point. This fact has been attributed to the high heat of fusion of silicon. The heat of fusion of silicon is much higher than that of aluminum (50.2kJ/mol silicon compare with 10.7kJ/mol aluminum) [8]. Therefore, this high heat release during

solidification enables the alloys with higher silicon to maintain the molten state longer and result in an increased flow distance. In hypoeutectic alloys, the heat of fusion of silicon is the most evident during eutectic solidification, when the Si phase formed. However, in hypereutectic alloys, the heat of fusion of silicon is also released during the formation of primary Si phase. Therefore, at the constant degree of superheat, the Al-Si alloys system exhibit the maximum fluidity at composition in excess of the eutectic.

*** Effect of temperature**

Figure 9 shows various aluminum silicon alloys increased with increasing pouring temperature. In the case of alloy without superheat, the nucleation of fine grains immediately at the tip. On the other hand, under superheat, nucleation is delayed and resulted in an increased fluidity length. So, superheat is the main factor that increases fluidity. The relationship between fluidity and temperature is considered a linear. In the vicinity of melting point, fluidity is not very good, but when superheat about 100^0C, the fluidity is very good, and in figure above shown the case even with superheat 150^0C.

We simplify the fluid flow problem somewhat by neglecting friction and acceleration effects and by assuming no separation of the flow stream occurs. Then, for constant applied head, velocity of the stream tip is a constant ν.

The total length of flow before the channel entrance solidifies is therefore:

$$L_f = t_f . v$$

$$t_f = \frac{\rho a f_s^c}{2h(T_M - T_0)}\left(H + c^{'}\Delta T\right)$$

where, L_f is fluidity

t_f: solidification time

ρ : density of liquid metal (Al = 2373kg/m^3)

h: heat transfer coefficient

a: channel radius

T_M: melting temperature

T_0: mold temperature

H: heat of fusion

c': specific heat of molten metal

ΔT: superheat.

f_s^c : fraction of solid criteria

Chapter 3

Experimental procedure

There are serveral types of fluidity test have been used by several investigators to measure the fluiditly of metal alloys. Vacuum fluidity test is advance method and adopted in this study. In order to easy the experiments, straight tubes set vertically was used instead of using bent horizontal tube.

3.1 Prepare alloys

Aluminum alloys were selected base on the wise use of it on market, as they are AC2B, AC4CH, AC4B, AC9A, ADC12 and ADC14. Hypoeutectic alloys AC2B, AC4CH and AC4B mainly used in case gravity casting to produce automobile and motorcycle parts. Hypereutectic alloys ADC12 and ADC14 are mainly for die casting. Chemical compositions of alloys used are list in table 2

3.2 Set up equipment system

Equipment used for fluidity test have been checked very well before set up and schematically shown in figure 8

3.3. Prepare mold materials

Stainless steel, copper and quartz served as mold materials. The stainless steel tubes were 500mm long, inside diameter 4.7mm and 6.35mm, respectively. Coper tubes were 500mm long, inside diameter 2mm, 3mm and 4mm, respectively. Quartz tubes were 500mm long with 3.5mm inside diameter.

First, the fluidity test tube were clean by blow compress air, after that rinsed with acid nitric 2% and then, perfect dried again just before use.

3.4 Experimental procedure

A vacuum was created by rotary vacuum pump with high accuraccy 0.1 torr by digital vacuum gauge. Pressure in reservoir chamber was adjusted by needle valve.

When reaching a predetermined temperature, the test tube were immersed into the molten metal to a depth of around 2.5cm (1 inch) and then needle valve opened to apply the vacuum to the fluidity test tube. The molten metal instantaneously sucks into the tube. The distance of the flowed liquid metal as measured from the surface of the molten metal in the crucible to the end of solidified fluidity test tube, as definition of fluidity.

In this study, operating variables were considered:

- Pouring temperature (or in term of superheat)
- Suction pressure (applied pressure and effective pressure)
- Mold materials (as mention above)

Fluidity test were examined at 5 different superheats: 0, 30, 60, 90 and 120K, respectively. In case of suction pressure, fluidity test were examined at 4 different pressures: 1.33 kPa, 2.67 kPa, 4.0 kPa and 6.67 kPa, respectively.

High vacuum 95 kPa were trial to investigate the different with low vacuum.

Horizontal fluidity test were also trial to compare with vertical fluidity test to understand the effect of gravity.

Table 2. Chemical compositions of alloys used in experiments

Alloys	Si	Fe	Cu	Ti	Mn	Mg	Ni	Zn	Ca	Sn	Pb
AC2B	5.97	0.80	2.36	0.01	0.26	0.28	0.13	0.03	0.005	0.00	0.01
AC4B	9.5	0.61	2.56	0.05	0.21	0.44	0.12	0.25	0.002	0.02	0.02
AC9A	22.83	0.30	1.26	0.03	0.14	1.28	0.96	0.05	0.002	0.00	0.01
ADC14	17.8	0.85	4.83	0.04	0.24	0.58	0.15	0.48	0.002	0.02	0.06
ADC12	11.2	0.64	1.88	0.04	0.11	0.16	0.05	0.66	-	0.02	-
AC4CH	7.14	0.14	0.40	0.07	0.00	0.25	0.05	0.00	-	0.02	-

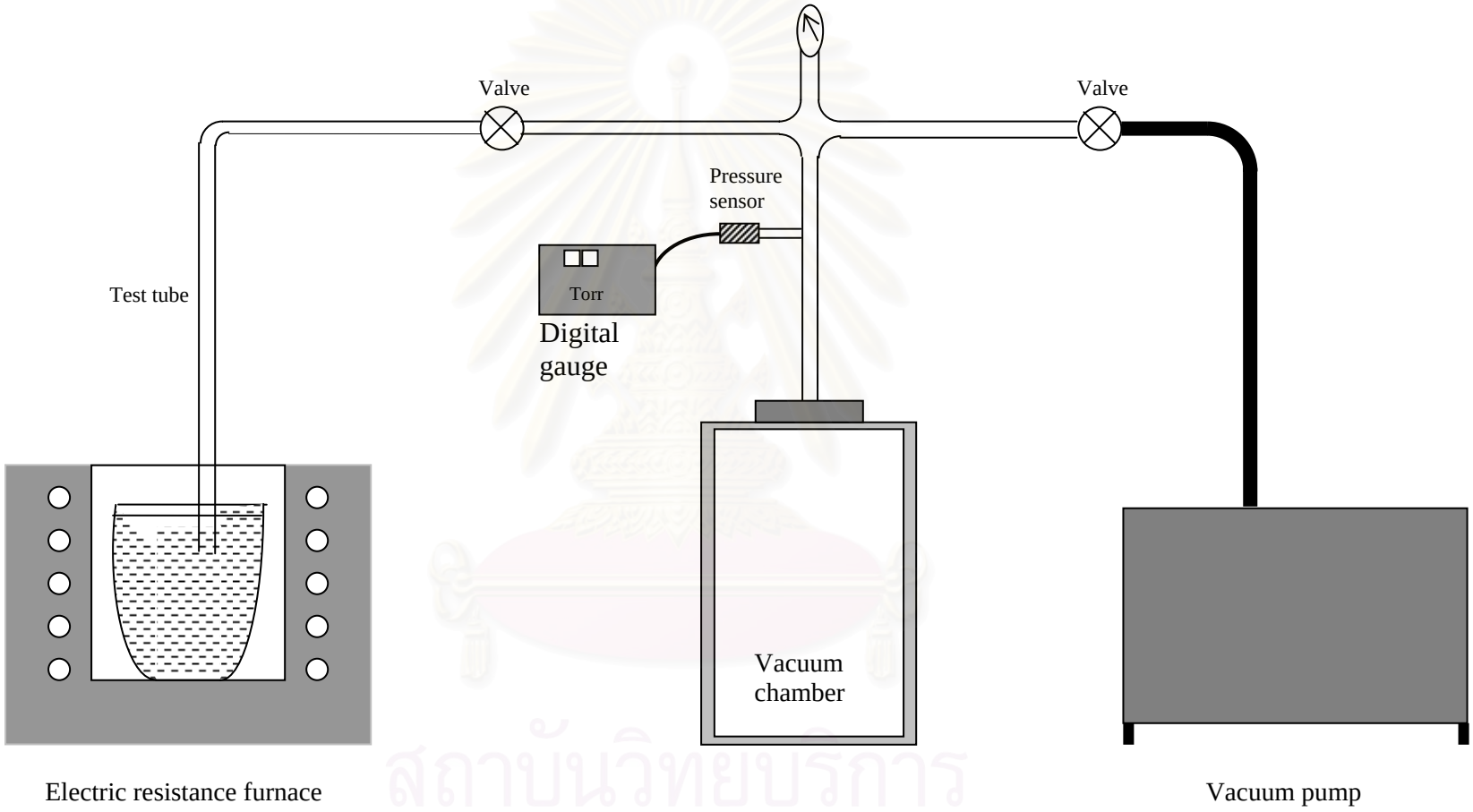

Figure 8. Schematic diagram of experimental equipment

Chapter 4

Experimental results

4.1 Fluidity of test alloys

The relationship between fluidity length and suction pressure at constant degree of superheat show in figure 9, figure 11, figure 13, figure 15 figure 17 and figure 19 of alloys AC2B, AC4CH, AC4B, ADC12 and ADC14, AC9A, respectively. As in table 2, silicon content in the range of 6 to 23%. For each alloy, the same experimental conditions are maintained: suction pressure and degree of superheat.

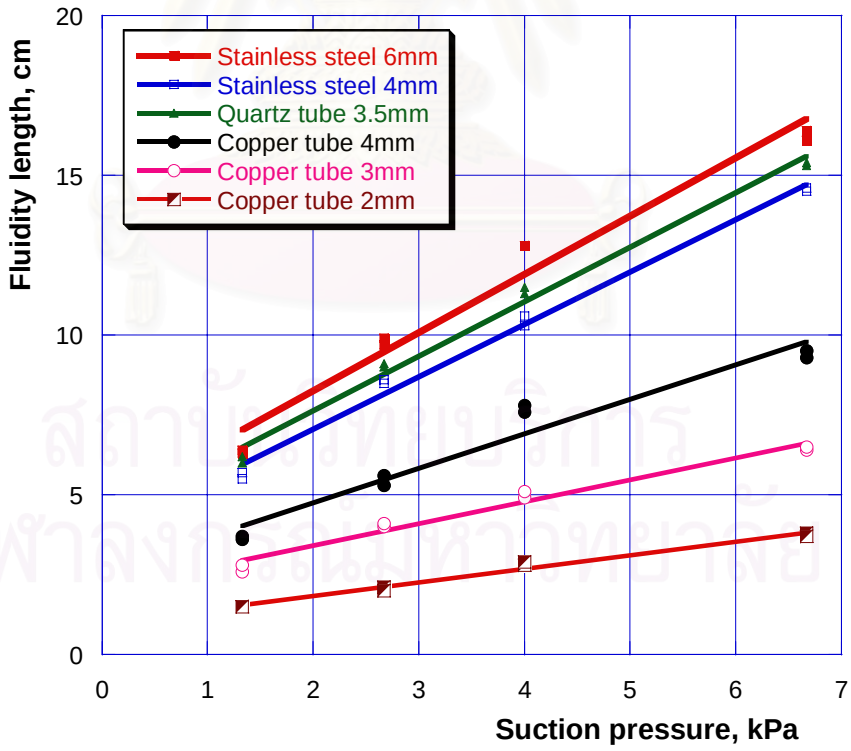

Figure 9. Relationship between fluidity and suction pressure at 973 K (ΔT = 85 K), alloy AC2B with liquidus temperature $T_L = 615^0C$ (888 K)

Table 3. Results of fluidity test of alloy AC2B

Suction pressure, kPa	Square root suction pressure, $Pa^{1/2}$	Stainless steel 6mm	Stainless steel 4mm	Quartz tube 3.5mm	Copper tube 4mm	Copper tube 3mm	Copper tube 2mm
1.33	36.5	6.3	5.5	6.0	3.6	2.6	1.5
1.33	36.5	6.4	5.7	6.2	3.7	2.8	1.5
2.67	51.5	9.7	8.5	9.0	5.3	4.0	2.1
2.67	51.5	9.9	8.6	9.1	5.6	4.1	2.0
4.0	63.2	12.8	10.3	11.3	7.6	4.9	2.8
4.0	63.2	12.8	10.6	11.5	7.8	5.1	2.9
6.67	82.0	16.1	14.5	15.3	9.3	6.4	3.8
6.67	82.0	16.4	14.6	15.4	9.5	6.5	3.7

Table 4. Results of fluidity test with different superheats, alloy AC2B

Superheat, Kelvin	Stainless steel 6mm	Stainless steel 4mm	Quartz tube 3.5mm	Copper tube 4mm	Copper tube 3mm	Copper tube 2mm
0	5.5	3.5	5.2	1.6	1.5	1.1
30	11.0	6.0	10.2	5.2	3.5	2.0
30	11.5	6.1	10.1	5.1	3.4	2.1
60	14.9	8.9	13.5	7.2	5.6	2.8
60	14.8	9.0	13.5	7.4	5.8	2.9
90	17.5	13.6	16.2	9.6	7.4	4.2
90	17.6	13.6	16.3	9.3	7.6	4.3

Stainless steel, copper and quartz were served as mold materials with the length of 500mm as a standard. Inner diameter was 4.7 mm and 6.35 mm for stainless steel, 2 mm, 3 mm, 4 mm for copper and 3.5 mm for quartz, respectively. The relationship is found linear as expected; higher fluidity is obtained by using a larger diameter tube. Stainless steel with 6.35mm inner diameter achieved the longest fluidity. And copper tube with 2 mm inner diameter achieved shortest fluidity. By dynamic of kinetic, this is reasonable. Digitals data show in tables 3, 5, 7, 9, 11, 13, respectively.

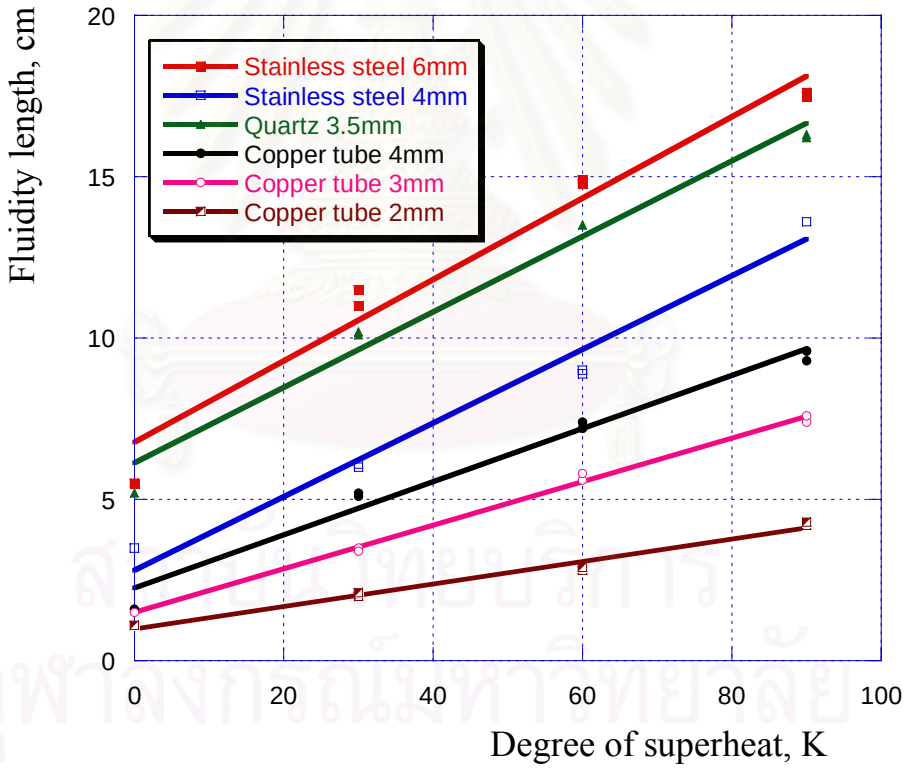

Figure 10. Relationship between fluidity and superheat at constant suction pressure 6.67kPa, alloy AC2B.

The relationship between fluidity and superheat at constant suction pressure 6.67kPa show in figures 9, 11, 13, 15, and 17 of alloys AC2B, AC4CH, AC4B, ADC12 and ADC14, respectively. In experimental of fluidity with different degree of superheats, stainless steel, copper and quartz were served as mold materials with the length of 500mm as a standard. Inner diameter was 4.7 mm and 6.35 mm for stainless steel, 2 mm, 3 mm, 4 mm for copper and 3.5 mm for quartz, respectively.

As expected, the higher superheat the longer fluidity length. From these figures, we can recognize that stainless steel tube in the group with its own slope, Copper tube in the group with its own slope. The degrees of superheat were up to 90 K, the condition closed to the real cases.

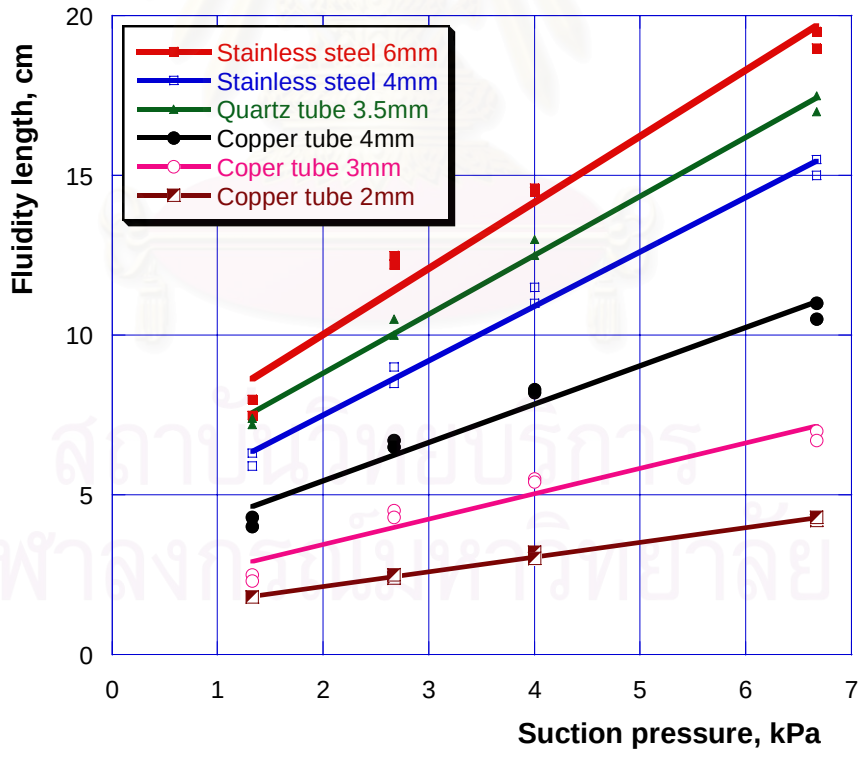

Figure 11. Relationship between fluidity and suction pressure at 973 K (ΔT = 85 K), alloy AC4CH. Liquidus temperature $T_L = 610^0$C (883 K).

Table 5. Results of fluidity test of alloy AC4CH

Suction pressure, kPa	Square suction pressure, $Pa^{1/2}$	Stainless steel 6mm	Stainless steel 4mm	Quartz tube 3.5mm	Copper tube 4mm	Copper tube 3mm	Copper tube 2mm
1.33	36.5	7.5	5.9	7.2	4.0	2.5	1.8
1.33	36.5	8.0	6.3	7.4	4.3	2.3	1.8
2.67	51.5	12.2	9.0	10.0	6.7	4.5	2.4
2.67	51.5	12.5	8.5	10.5	6.5	4.3	2.5
4.0	63.2	14.5	11.5	12.5	8.3	5.5	3.2
4.0	63.2	14.6	11.0	13.0	8.2	5.4	3.0
6.67	82.0	19.0	15.5	17.0	10.5	7.0	4.2
6.67	82.0	19.5	15.0	17.5	11.0	6.7	4.3

Table 6. Results of fluidity test with different superheats, alloy AC4CH

Superheat, Kelvin	Stainless steel 6mm	Stainless steel 4mm	Quartz tube 3.5mm	Copper tube 4mm	Copper tube 3mm	Copper tube 2mm
0	6.0	4.0	5.0	2.0	1.5	1.0
30	11.8	6.5	10.5	5.4	3.2	2.5
30	12.0	6.8	10.8	5.2	3.5	2.4
60	16.2	10.1	14.3	7.2	5.4	3.5
60	16.0	10.3	14.5	7.3	5.7	3.6
90	19.0	14.3	17.1	8.5	7.0	5.0
90	19.5	14.5	17.4	8.7	6.7	5.1

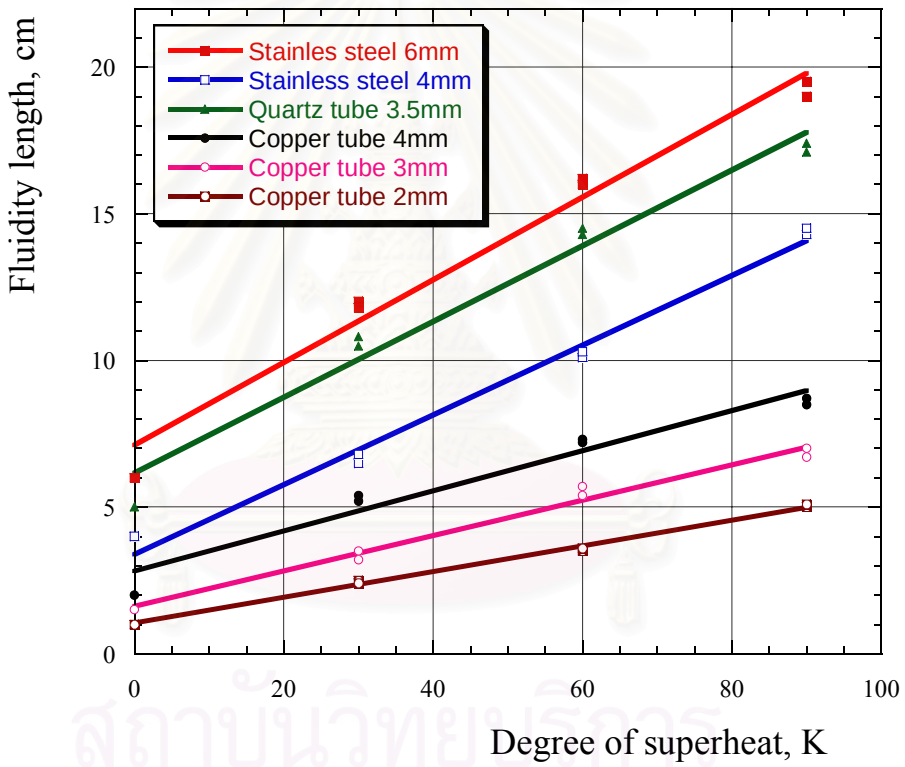

Figure 12. Relationship between fluidity and superheat at constant suction pressure 6.67 kPa, alloy AC4CH.

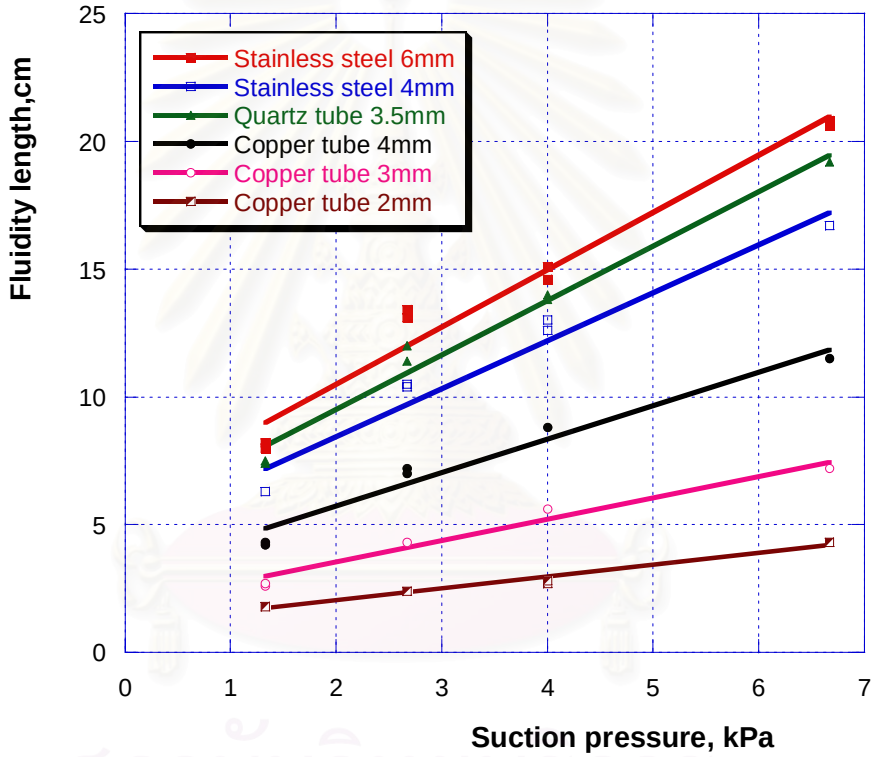

Figure 13. Relationship between fluidity and suction pressure at 973 K (ΔT = 110 K) alloy AC4B with liquidus temperature T_L = 590^{0}C (863 K)

Table 7. Results of fluidity test of alloy AC4B

Suction pressure, kPa	Square suction pressure, $Pa^{1/2}$	Stainless steel 6mm	Stainless steel 4mm	Quartz tube 3.5mm	Copper tube 4mm	Copper tube 3mm	Copper tube 2mm
1.33	36.5	8.0	6.3	7.4	4.2	2.6	1.8
1.33	36.5	8.2	6.3	7.5	4.3	2.7	1.8
2.67	51.5	13.4	10.4	12.0	7.0	4.3	2.4
2.67	51.5	13.1	10.5	11.4	7.2	4.3	2.4
4.0	63.2	14.6	13.0	14.0	8.8	5.6	2.7
4.0	63.2	15.1	12.6	13.8	8.8	5.6	2.8
6.67	82.0	20.8	16.7	19.2	11.5	7.2	4.3
6.67	82.0	20.6	16.7	19.2	11.5	7.2	4.3

Table 8. Results of fluidity test with different superheats, alloy AC4B

Superheat, Kelvin	Stainless steel 6mm	Stainless steel 4mm	Quartz tube 3.5mm	Copper tube 4mm	Copper tube 3mm	Copper tube 2mm
0	6.4	5.1	5.4	4.1	2.8	1.0
30	11.5	8.0	10.3	6.2	4.0	2.1
30	11.5	8.0	10.4	6.2	4.3	2.2
60	15.0	10.0	13.2	8.0	5.1	3.5
60	15.0	10.0	13.2	8.1	5.2	3.5
90	19.1	14.1	17.8	10.2	6.0	4.0
90	19.1	13.8	17.8	10.2	6.5	3.9
110	20.8	16.7	19.2	11.5	7.2	4.3
110	20.6	16.7	19.2	11.3	7.2	4.3

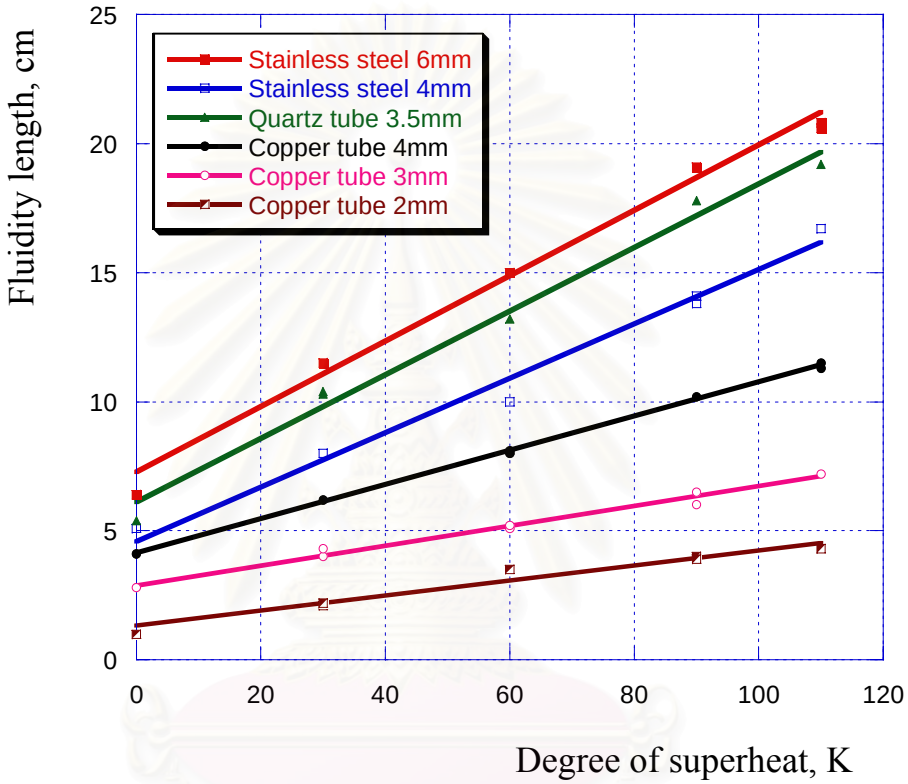

Figure 14. Relationship between fluidity and superheat at constant suction pressure 6.67 kPa, alloy AC4B

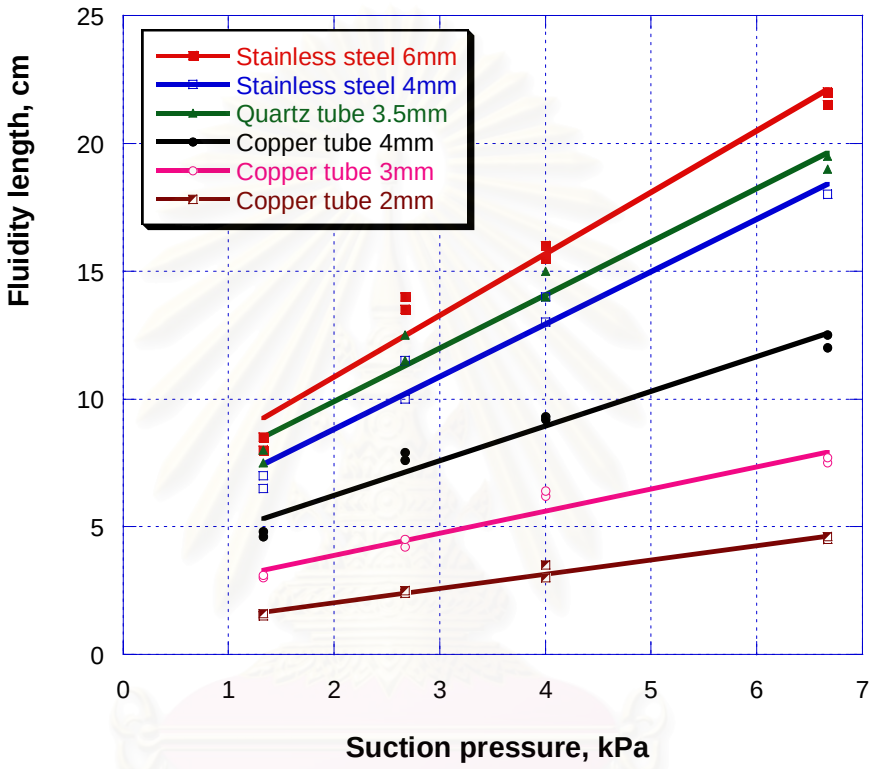

Figure 15. Relationship between fluidity and suction pressure at 973 K (ΔT = 120 K) alloy ADC12 with liquidus temperature T_{L} = 580^{0}C (853 K).

Table 9. Results of fluidity test of alloy ADC12

Suction pressure, kPa	Square suction pressure, $Pa^{1/2}$	Stainless steel 6mm	Stainless steel 4mm	Quartz tube 3.5mm	Copper tube 4mm	Copper tube 3mm	Copper tube 2mm
1.33	36.5	8.0	6.5	7.5	4.6	3.0	1.5
1.33	36.5	8.5	7.0	8.0	4.8	3.1	1.6
2.67	51.5	13.5	10.0	11.5	7.9	4.2	2.4
2.67	51.5	14.0	11.5	12.5	7.6	4.5	2.5
4.0	63.2	15.5	13.0	14.0	9.2	6.2	3.5
4.0	63.2	16.0	14.0	15.0	9.3	6.4	3.0
6.67	82.0	21.5	18.0	19.0	12.0	7.5	4.5
6.67	82.0	22.0	18.0	19.5	12.5	7.7	4.6

Table 10. Results of fluidity test with different superheats, alloy ADC12

Superheat, Kelvin	Stainless steel 6mm	Stainless steel 4mm	Quartz tube 3.5mm	Copper tube 4mm	Copper tube 3mm	Copper tube 2mm
0	7.0	5.0	6.0	4.6	3.0	1.5
30	10.6	8.0	9.1	7.0	4.7	3.6
30	10.5	8.2	9.4	7.6	4.5	3.5
60	13.5	9.8	12.4	8.3	5.8	4.6
60	14.0	9.7	12.6	8.5	5.7	4.5
90	18.2	13.3	16.4	10.0	6.4	5.5
90	18.6	13.2	16.4	10.3	6.6	5.0
120	22.0	14.6	19.5	12.0	7.5	6.4
120	21.5	14.8	19.8	12.5	7.7	6.7

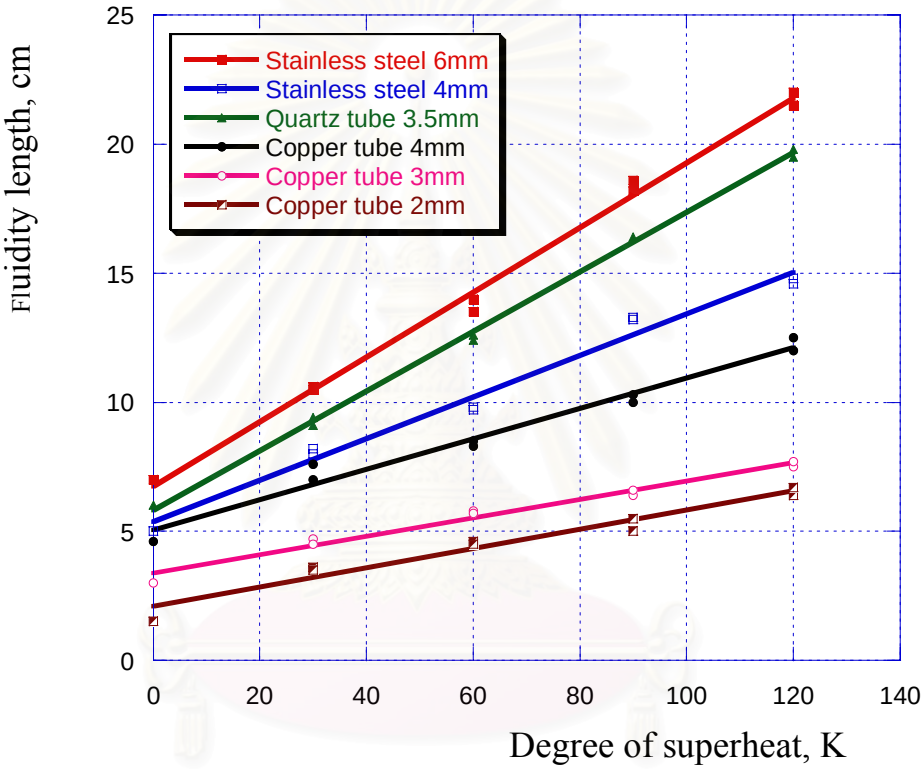

Figure 16. Relationship between fluidity and superheat at constant suction pressure 6.67 kPa, alloy ADC12

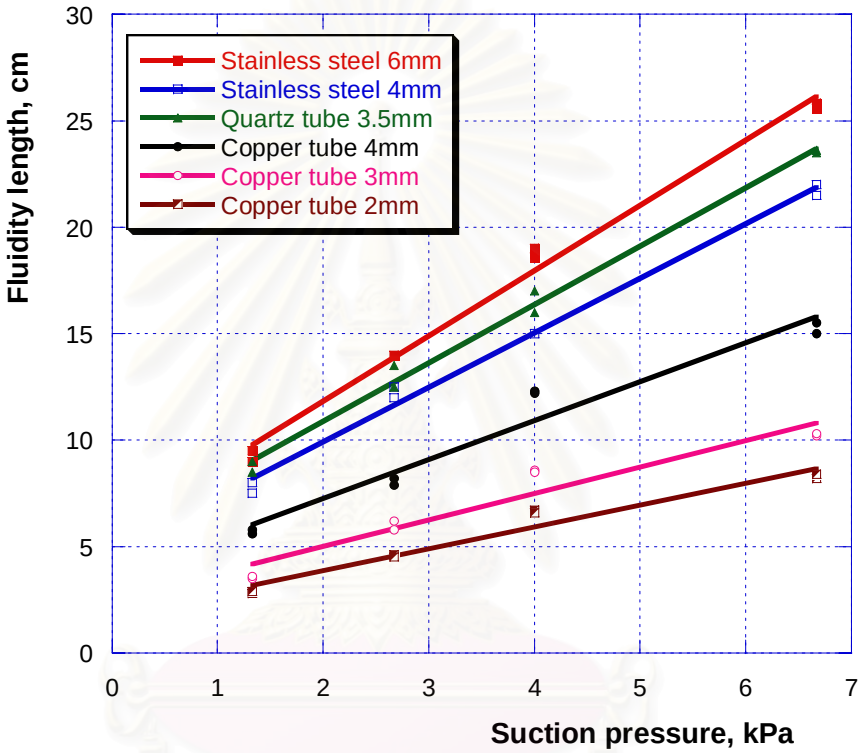

Figure 17. Relationship between fluidity and suction pressure at 973 K (ΔT = 60 K) alloy ADC14 with liquidus temperature $T_L = 640^0$C (913 K).

Table 11. Results of fluidity test of alloy ADC14

Suction pressure, kPa	Square root suction pressure, $Pa^{1/2}$	Stainless steel 6mm	Stainless steel 4mm	Quartz tube 3.5mm	Copper tube 4mm	Copper tube 3mm	Copper tube 2mm
1.33	36.5	9.0	7.5	8.5	5.6	3.5	2.8
1.33	36.5	9.5	8.0	9.0	5.8	3.6	2.9
2.67	51.5	14.0	12.0	12.5	7.9	5.8	4.6
2.67	51.5	14.0	12.5	13.5	8.2	6.2	4.5
4.0	63.2	18.6	15.0	16.0	12.2	8.6	6.7
4.0	63.2	19.0	15.0	17.0	12.3	8.5	6.6
6.67	82.0	25.6	21.5	23.6	15.0	10.2	8.2
6.67	82.0	25.8	22.0	23.5	15.5	10.3	8.4

Table 12. Results of fluidity test with different superheats, alloy ADC14

Superheat, Kelvin	Stainless steel 6mm	Stainless steel 4mm	Quartz tube 3.5mm	Copper tube 4mm	Copper tube 3mm	Copper tube 2mm
0	11.5	9	10.5	8	6.9	5.6
30	19	15.4	17.3	11.4	8.6	7.3
30	19	15.5	17.3	11.5	8.8	7.5
60	27.5	21.5	23.6	14.5	10.2	8.2
60	27.5	21.5	23.5	14	10.2	8.4

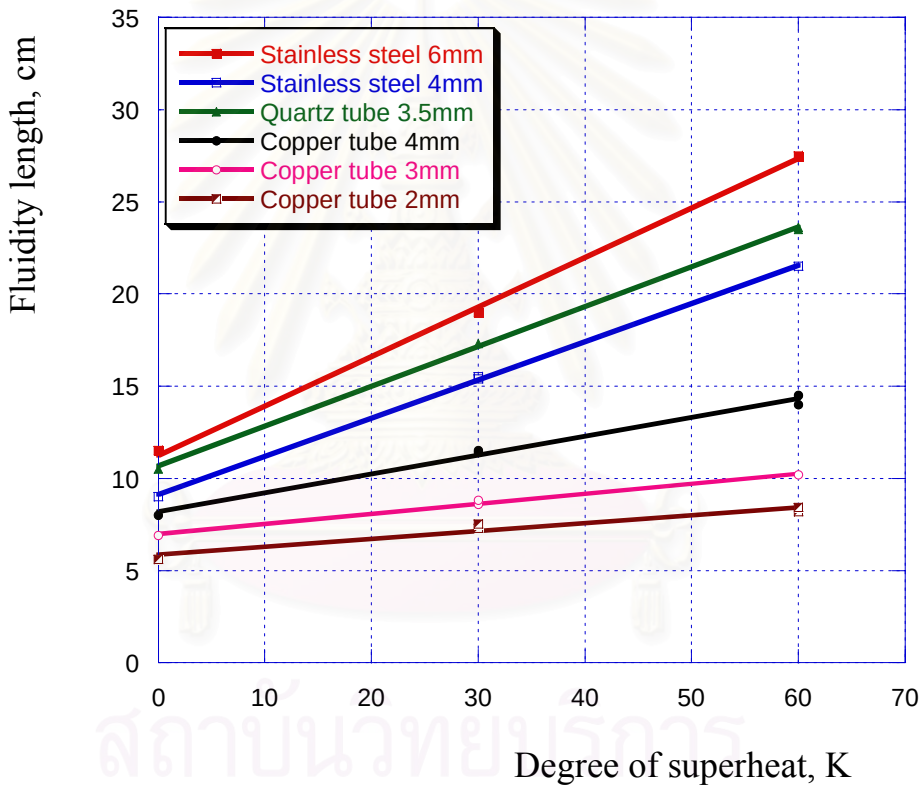

Figure 18. Relationship between fluidity and superheat at constant suction pressure 6.67 kPa, alloy ADC14

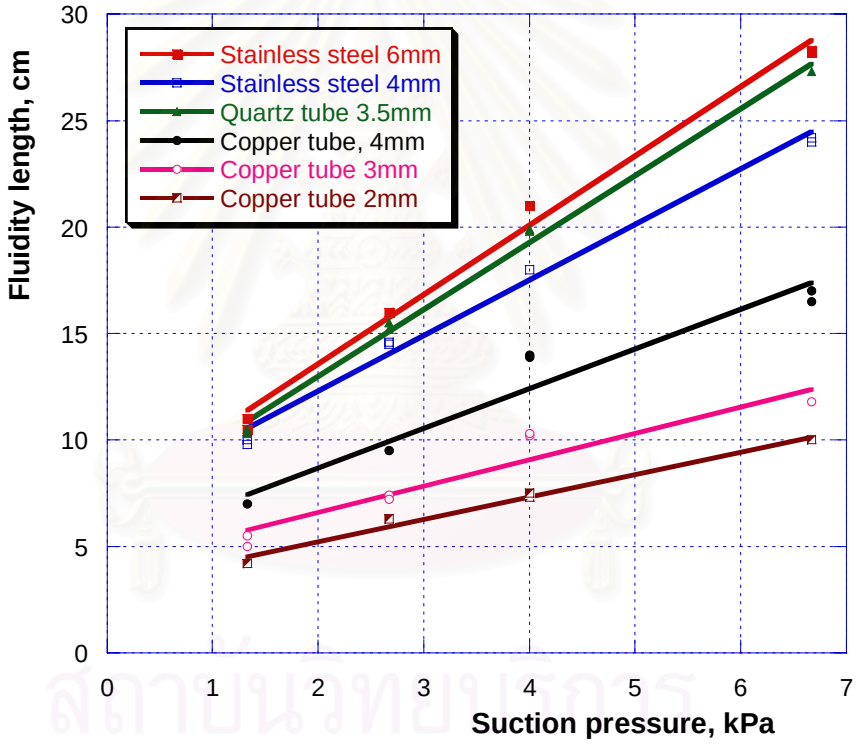

Figure 19. Relationship between fluidity and suction pressure at 1073 K (ΔT = 60 K) alloy AC9A with liquidus temperature T_L = 740 ^{0}C (1013 K).

Table 13. Results of fluidity test of alloy AC9A

Suction pressure, kPa	Square root suction pressure, $Pa^{1/2}$	Stainless steel 6mm	Stainless steel 4mm	Quartz tube 3.5mm	Copper tube 4mm	Copper tube 3mm	Copper tube 2mm
1.33	36.50	10.50	10.00	10.30	7.00	5.00	4.20
1.33	36.50	11.00	9.80	10.50	7.00	5.50	4.20
2.67	51.50	16.00	14.60	15.20	9.50	7.40	6.30
2.67	51.50	16.00	14.50	15.50	9.50	7.20	6.30
4.00	63.20	21.00	18.00	19.80	14.00	10.20	7.30
4.00	63.20	21.00	18.00	19.90	13.90	10.30	7.50
6.67	82.00	28.20	24.00	27.30	16.50	11.80	10.00
6.67	82.00	28.30	24.20	27.30	17.00	11.80	10.00

Table 14. Results of fluidity test with different superheats, alloy AC9A

Superheat, Kelvin	Stainless steel 6mm	Stainless steel 4mm	Quartz tube 3.5mm	Copper tube 4mm	Copper tube 3mm	Copper tube 2mm
0	12.5	10.0	11.5	9.0	7.9	6.6
30	20.0	16.7	18.3	12.4	9.6	8.3
30	20.0	16.5	18.3	12.5	9.8	8.5
60	29.0	22.5	24.6	15.5	11.2	9.2
60	29.0	22.5	24.5	15.0	11.2	9.4

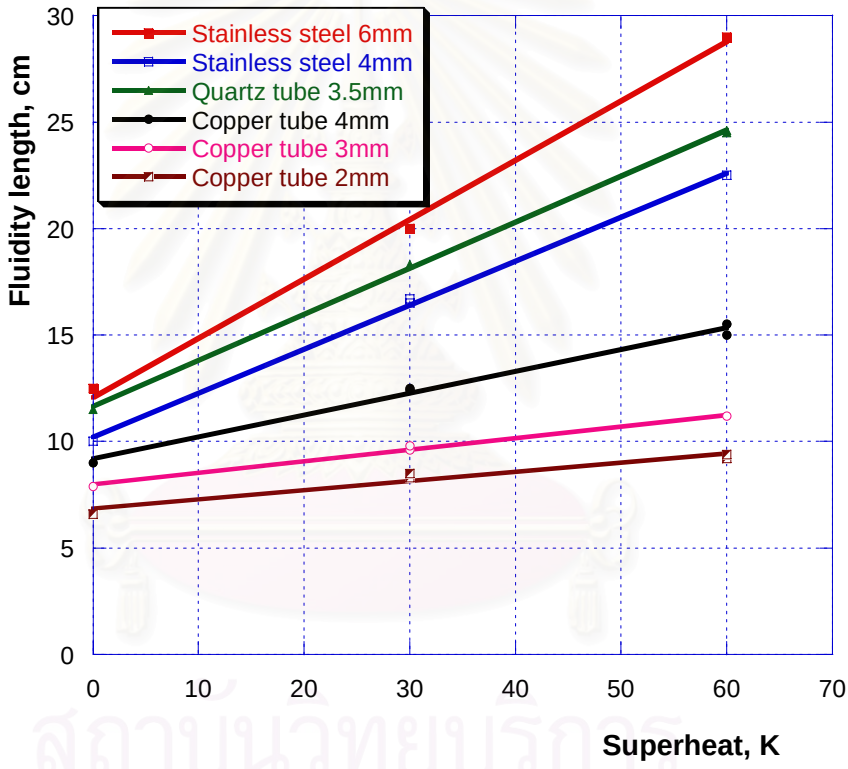

Figure 20. Relationship between fluidity and superheat at constant suction pressure 6.67 kPa, alloy AC9A

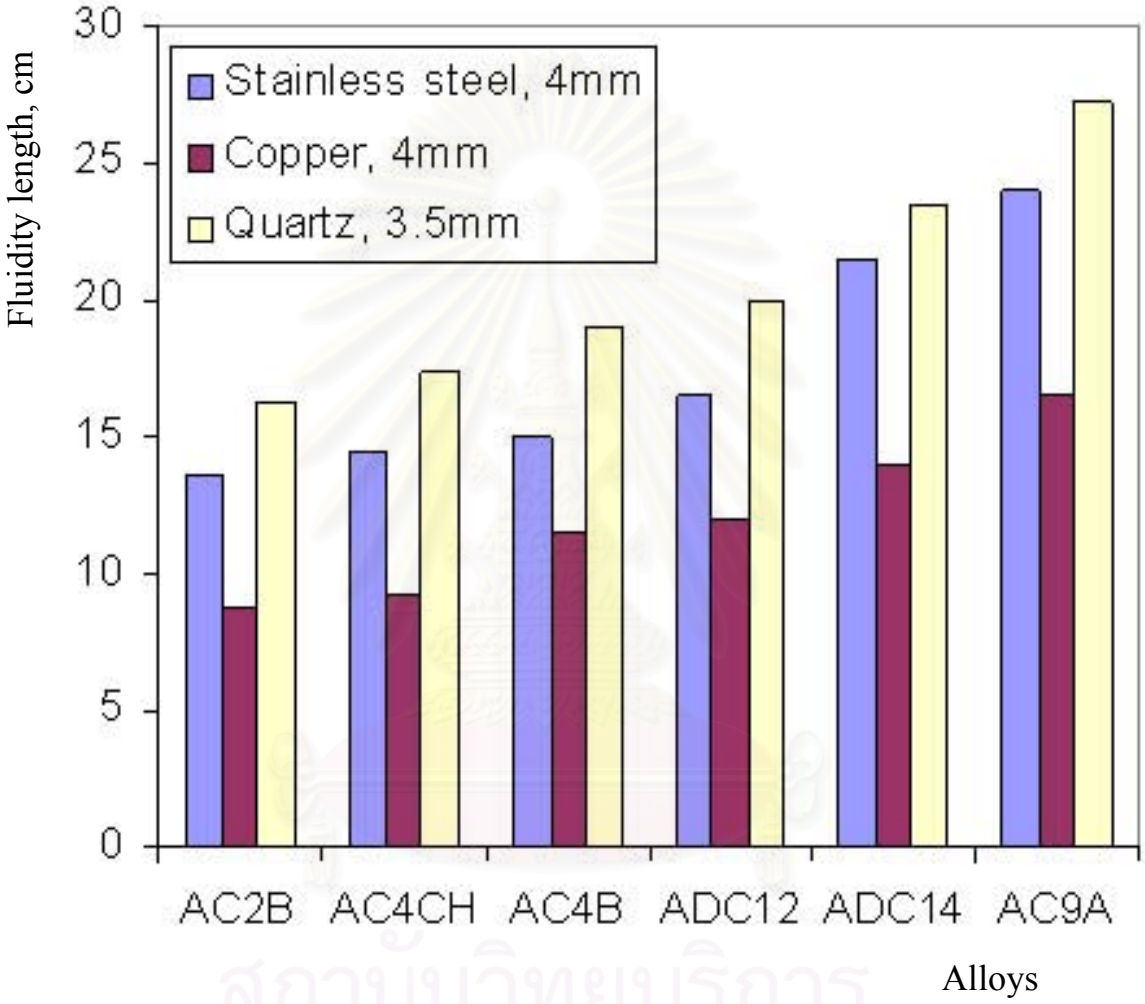

Figure 21. Ranking fluidity of aluminum alloys with superheat ΔT = 90 K, suction pressure is 6.67 kPa.

4.2 Microstructure of aluminum alloys in fluidity test

Figure 19 shows microstructure of aluminum alloy AC4CH with grains and dendrites structure. Figure 20 shows equiaxed structure. Figure 22 show well developed of intermetallic phase with aluminum matrix.

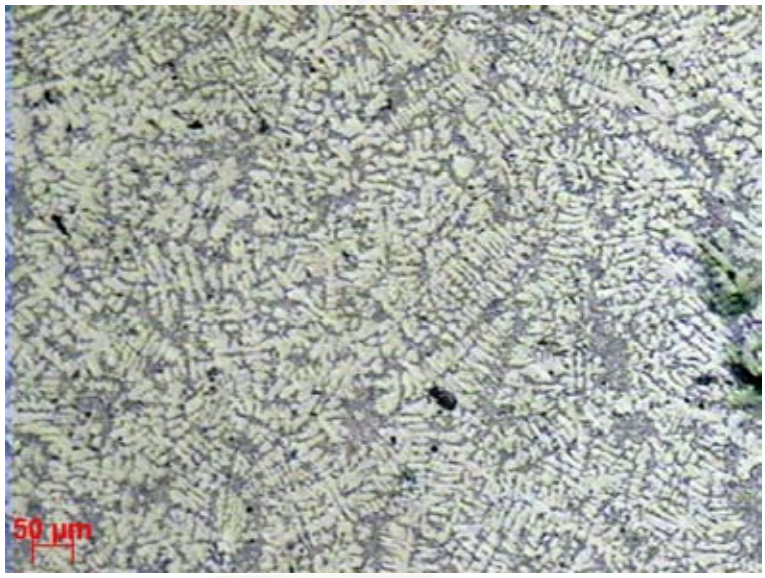

Figure 22. Microstructure of alloy AC4CH at the tip of fluidity test

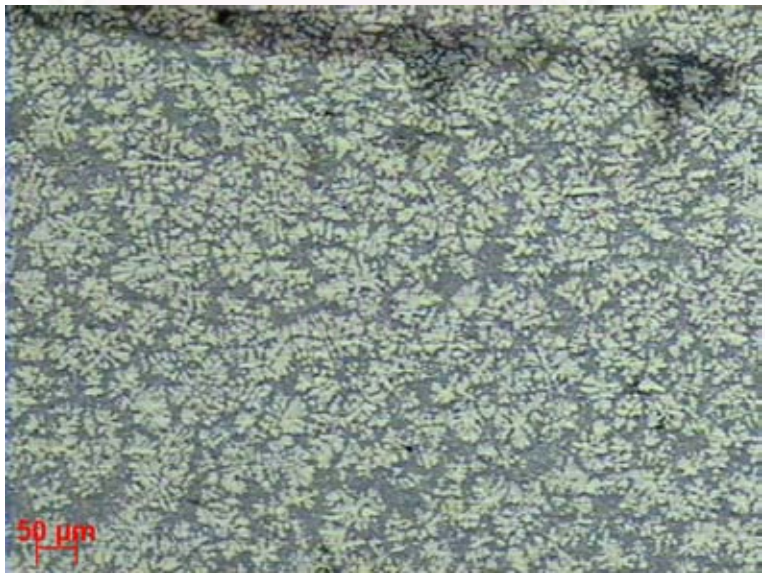

Figure 23. Microstructure of alloy AC4CH at the middle of fluidity test

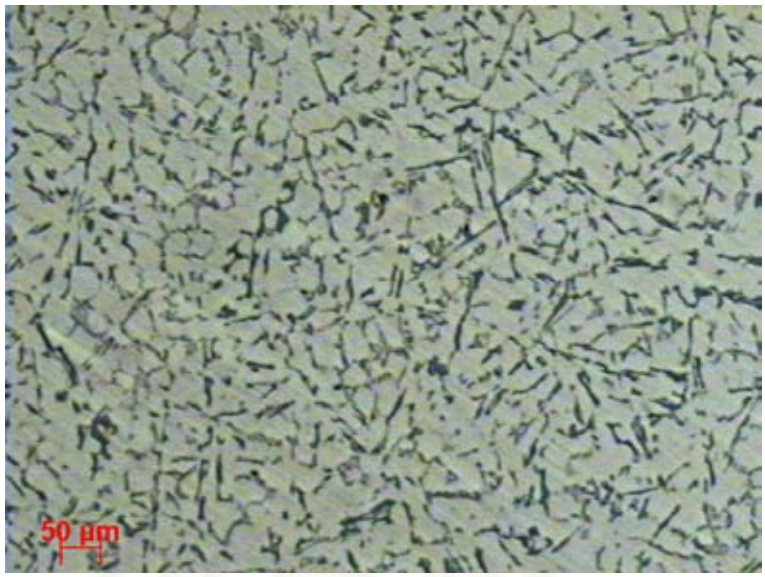

Figure 24. Microstructure of alloy AC4CH at the entrance fluidity test Magnification 5X.

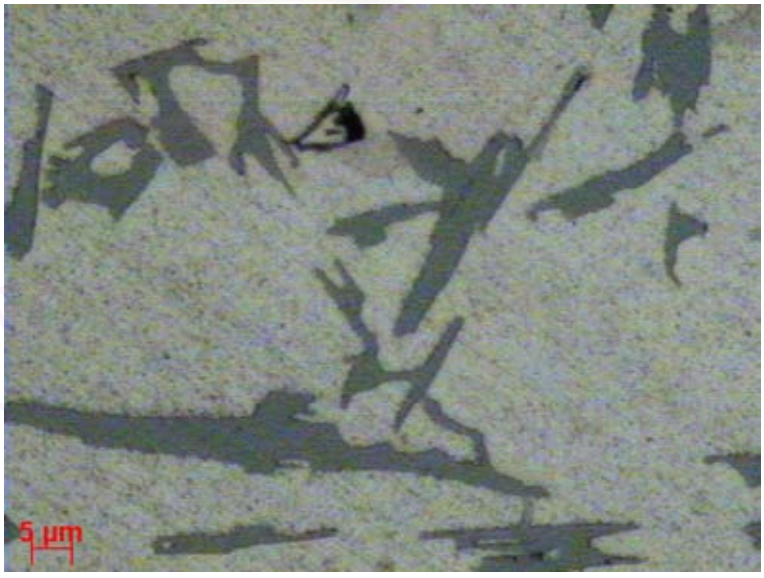

Figure 25. Microstructure of alloy AC4CH at the entrance fluidity test Magnification 50X.

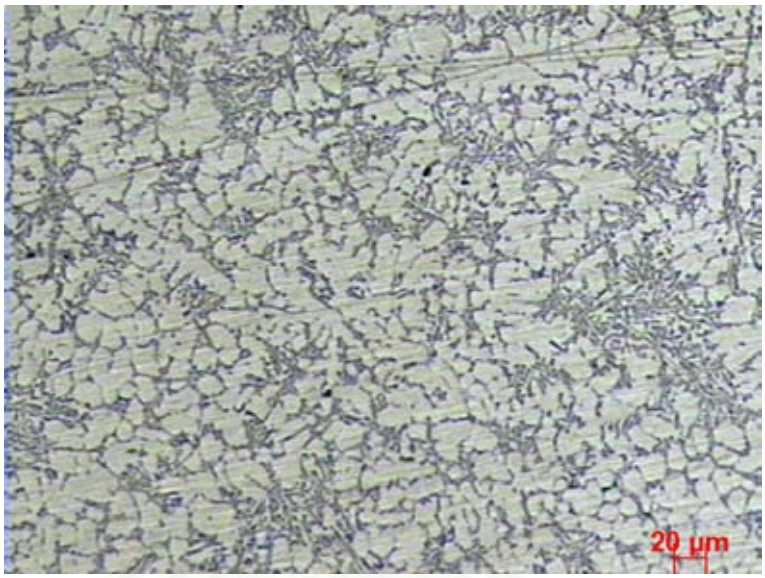

Figure 26. Microstructure of alloy ADC12 at the tip of fluidity test

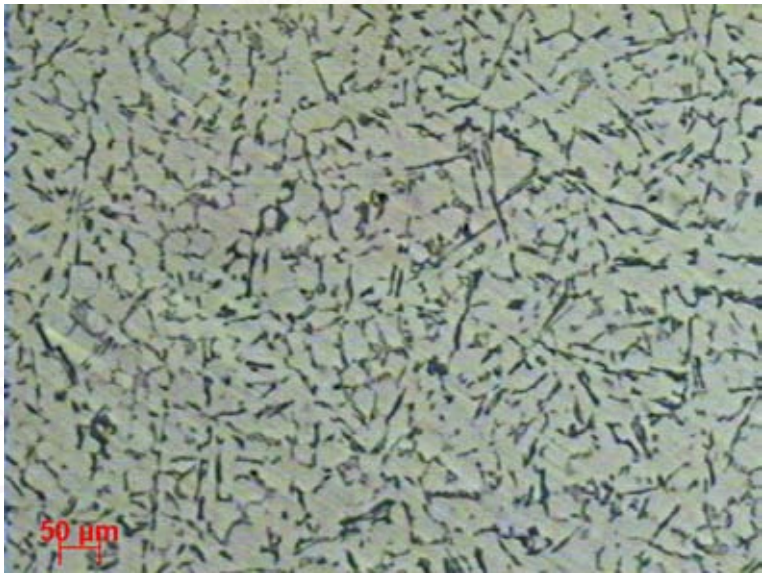

Figure 27. Microstructure of alloy ADC12 at the entrance fluidity test

Chapter 5

Discussion

5.1 Fluidity of test alloys

Aluminum silicon alloys were investigated at different suction pressure and degrees of superheat. Figure 27 shows relationships between fluidity and suction pressure of alloy AC4CH at temperature 973 K (700 ^{0}C).

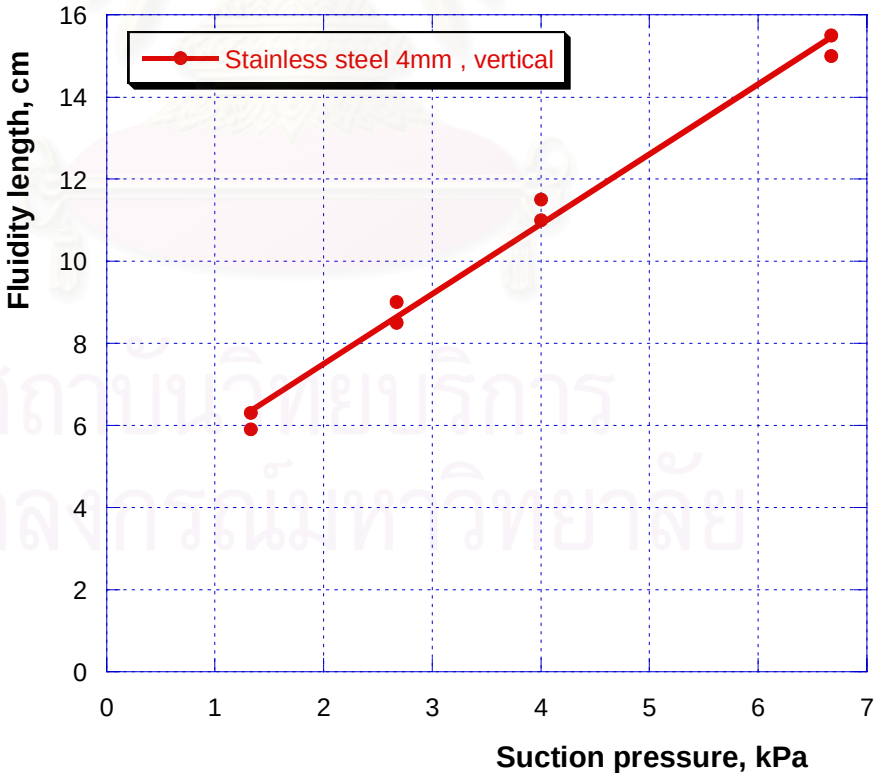

Figure 27. Relationship between fluidity and suction pressure, alloy AC4CH,

Liquid aluminum is sucked into stainless steel under pressure. At the entrance of the tube, velocity is maximum ν, but at the end of the tube (when liquid aluminum stopped) velocity equal 0. Therefore, the velocity of liquid aluminum inside tube can be estimate by average velocity $\bar{v}$. In vacuum fluidity test, it is clear that the origin force suck liquid aluminum is called "applied suction pressure" ΔP_a. From kinetic equation, we know the force that sucks liquid aluminum ΔP_a is proportional to kinetic energy

$$\Delta P_a \propto \frac{1}{2}\rho v^2$$

From equation above, we can reverse and get

$$v \propto \sqrt{\Delta P_a}$$

As mention in Chapter 2 fluidity length can calculate by multiply velocity and fluid time t_f

$$L = vt_f$$

Combination these equations, we obtained the final relationship: Fluidity length proportional to square root of applied suction pressure.

$$L \propto \sqrt{\Delta Pa}$$

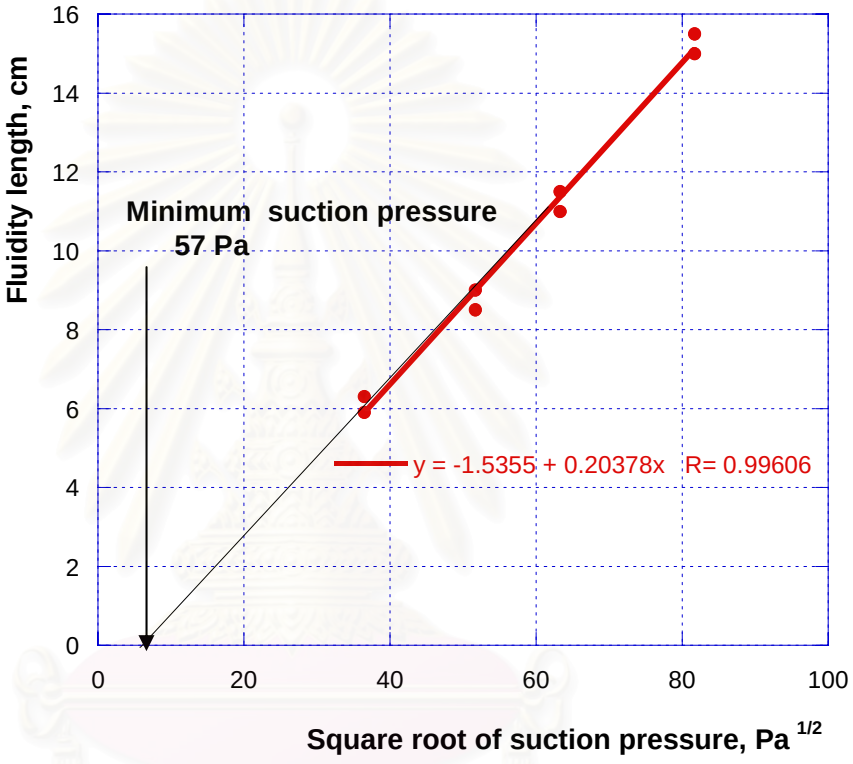

Figure 28. Relationship between fluidity and square root of suction pressure, alloy AC4CH,

Figure 28 shows relationship between fluidity length and square root of suction pressure. From this figure, extrapolate the relationship line cuts horizontal axis at some value, called “minimum applied suction pressure”. This is minimum value necessary in order to suck liquid aluminum. This value incase alloy AC4CH, at temperature 973 K, is 57 Pa. For different alloys, this value is changing in the range of 40 to 200 Pa

Applied suction pressure ΔP_a is expressed:

$$\Delta P_a = \Delta P_e + \rho g L + 4\sigma/D,$$

where ΔP_e: effective suction pressure; ρ: density; g: gravity acceleration constant; L: fluidity length; σ: surface energy; and D: tube diameter.

In this study, horizontal fluidity test is done with the maximum of fluidity length of about 30 cm. So, we can neglect the effect of back pressure by gravity ρgL.

Applied suction pressure distribute in 3 terms. The third term is called “surface tension” (or surface energy). This term causes negative effect to fluidity because surface tension will against fluid flow into test channel. The second term is called “back pressure by gravity”. This term causes negative effect to fluidity by fluidity length. Last, the first term is called “effective pressure”. This is really necessary pressure need to suck liquid aluminum. Effective pressure relates directly to “applied suction pressure”. As discuss before, fluidity length relates to square root of applied suction pressure. Therefore, fluidity length relates to square root of effective pressure also. Figure 29 show relationship between fluidity length and square root of effective pressure. This relationship is found linear. From the meaning of “effective pressure” we can see that, when “effective pressure” equal 0, the fluidity length is 0 also. It means that the relationship curve between square root of effective pressure and fluidity length pass through the origin. But in fact, this line did not pass origin. This can be understood if we look back to the equation of applied suction pressure. When calculating, value of surface tension using must be different with different alloys. The value of surface tension of pure aluminum is 0.9 (N/m).

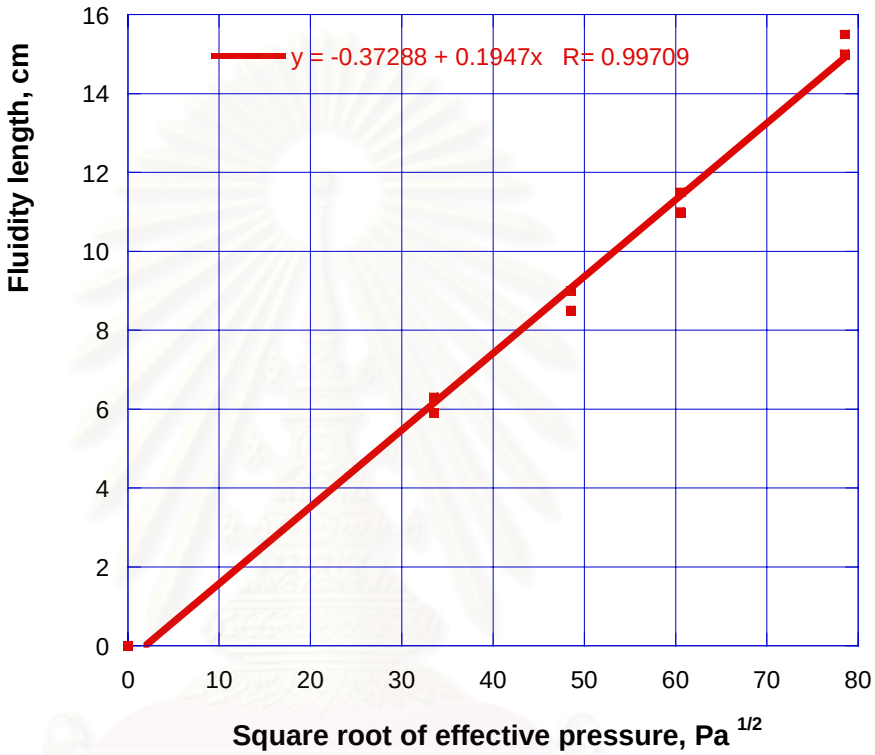

Figure 29. Relationship between fluidity and square root of effective pressure, alloy AC4CH,

By best fit value of surface tension, we get the relationship with the curve pass through the origin. By this calculation, value obtained for alloy AC4CH is $\sigma = 1.15$ (N/m)

In this research, experiments are done with several types of mold materials: stainless steel, copper tube, and quartz tube. The relationship between fluidity length and square root of suction pressure is shown in figure 29 to figure 35 of alloy AC4CH, AC2B. AC4B, ADC12, ADC14, AC9A, respectively.

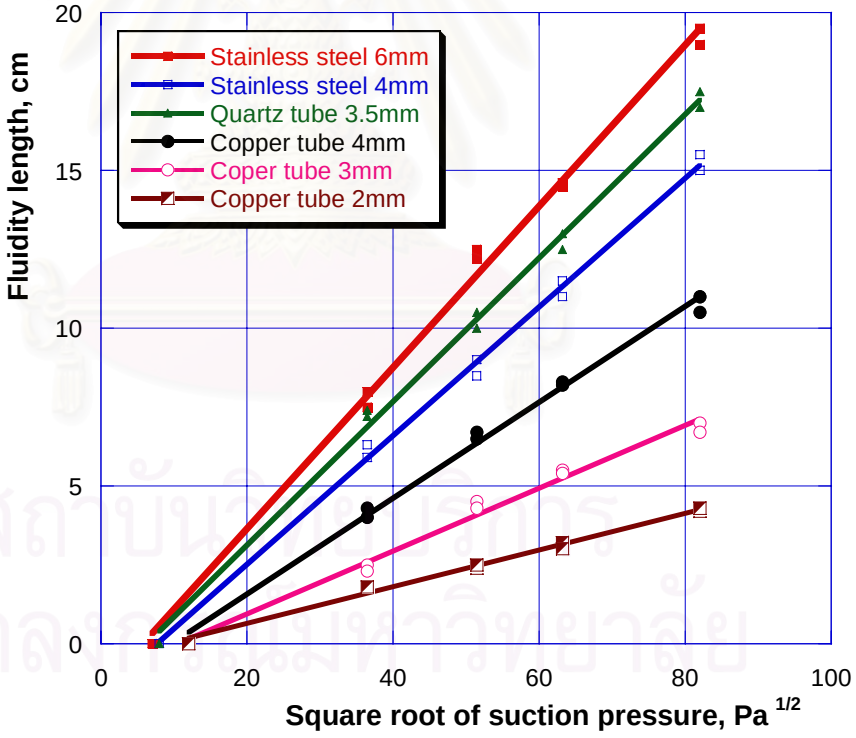

Figure 30. Relationship between fluidity and square root of suction pressure at 973 K (ΔT = 85 K), alloy AC4CH. Liquidus temperature $T_L = 610^0C$ (883 K).

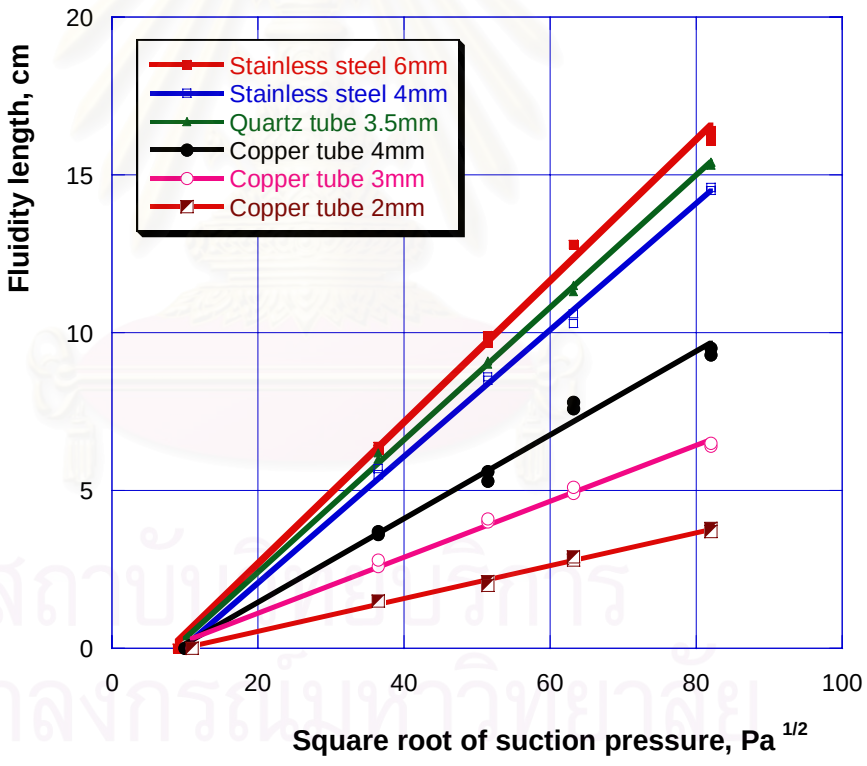

Figure 31. Relationship between fluidity and square root of suction pressure at 973 K ($\Delta T = 85^0C$), alloy AC2B with liquidus temperature $T_L = 615^0C$ (888 K)

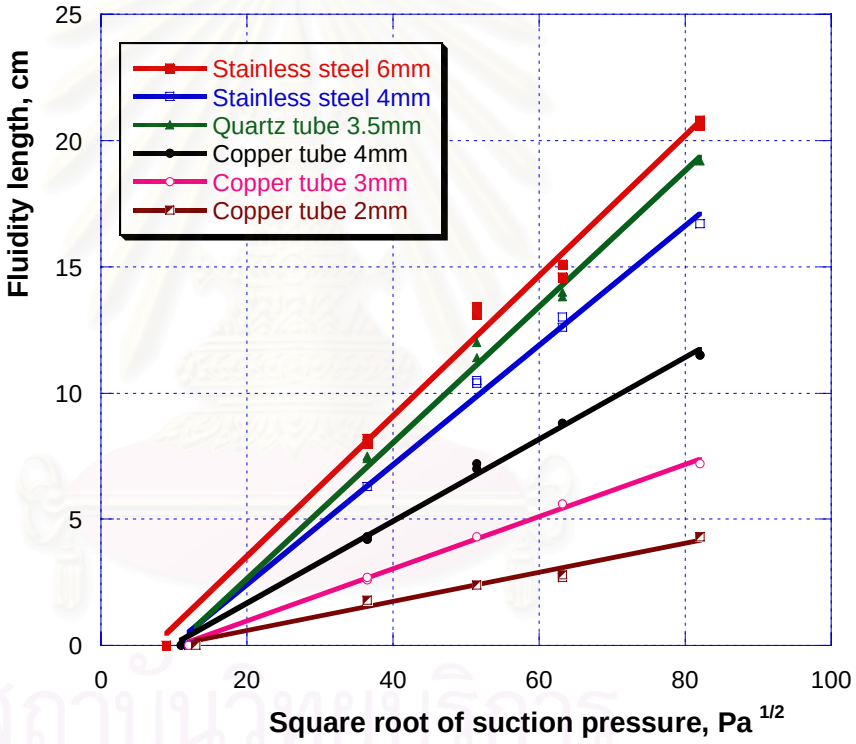

Figure 32. Relationship between fluidity and square root of suction pressure at 973 K (ΔT = 110 K) alloy AC4B with liquidus temperature $T_{L=}590^{0}$C (863 K)

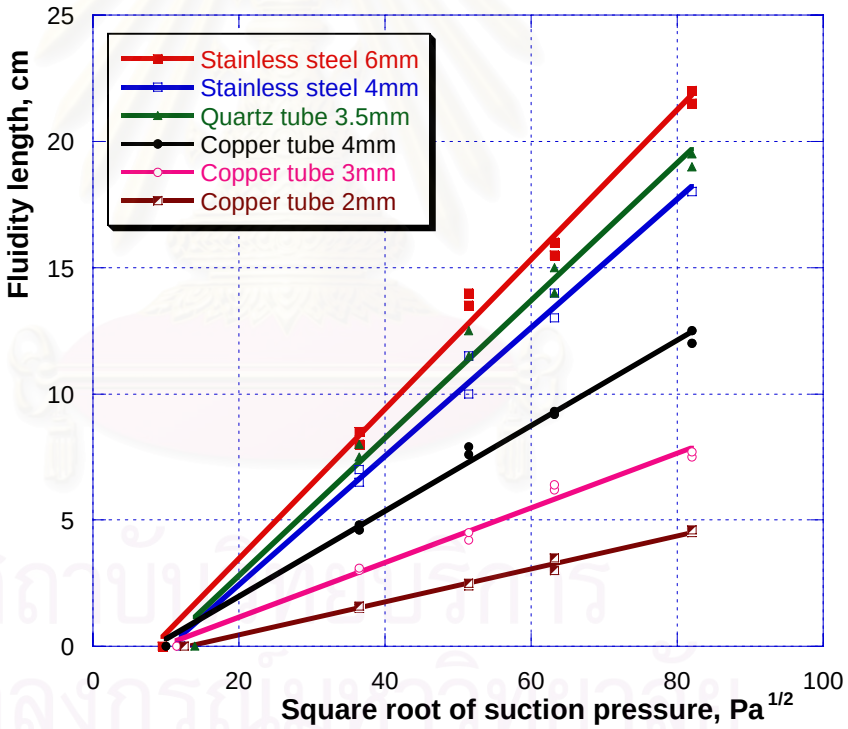

Figure 33. Relationship between fluidity and square root of suction pressure at 973 K (ΔT = 120 K) alloy ADC12 with liquidus temperature $T_{L} = 580^{0}$C (853 K).

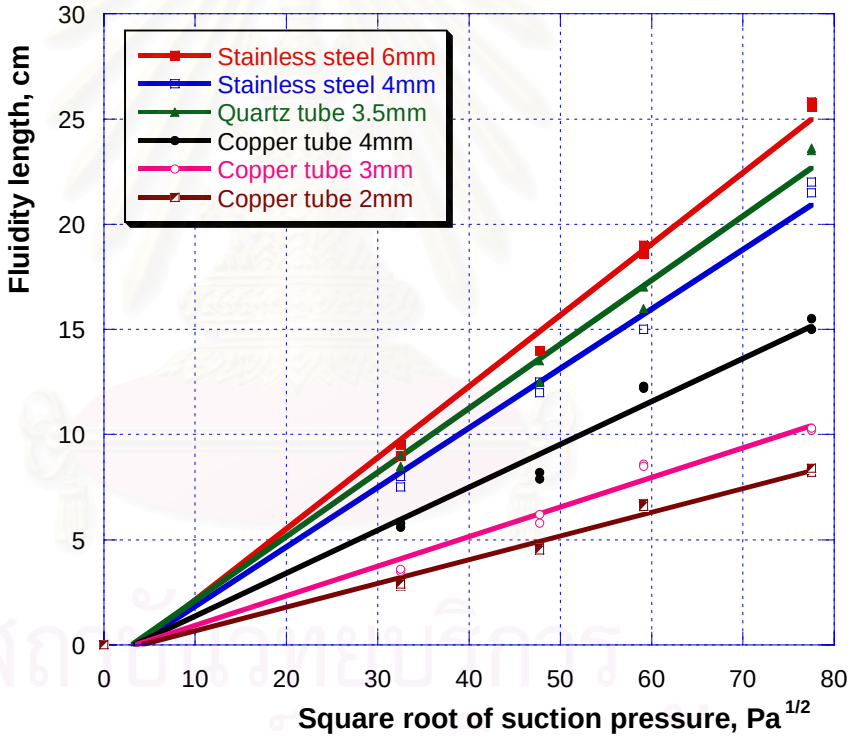

Figure 34. Relationship between fluidity and square root of suction pressure at 873 K (ΔT = 60 K) alloy ADC14 with liquidus temperature $T_{L} = 640^{0}$C (913 K).

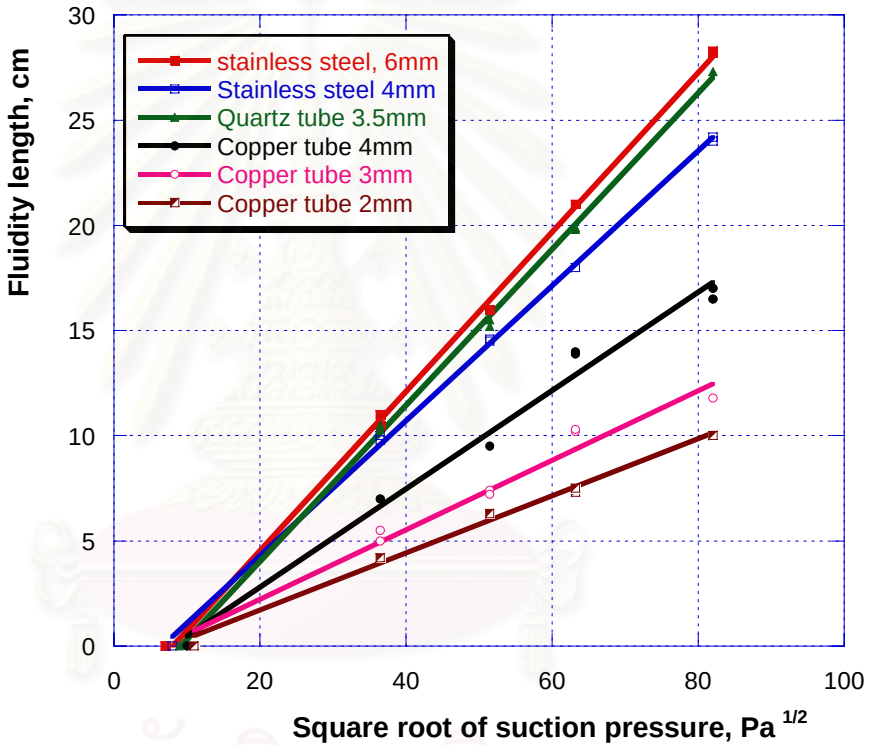

Figure 35. Relationship between fluidity and square root of suction pressure at 1073 K (ΔT = 60 K) alloy AC9A with liquidus temperature $T_L = 740^0$C (1013 K).

In these experiment conditions, solidification is rate-determined by the heat transfer between the mold and casting. According to Niyama *et al*. the order of heat conductivity is 395 W/(m.K) for copper, 16.5 W/(m.K) for stainless steel, and 1.9 W/(m.K) for quartz. Therefore, from the fluidity difference, a characteristic heat transfer coefficient between each mold and alloy exists. In figure 10 shows relation between fluidity length and suction pressure at constant degree superheat 90 K of AC4CH.

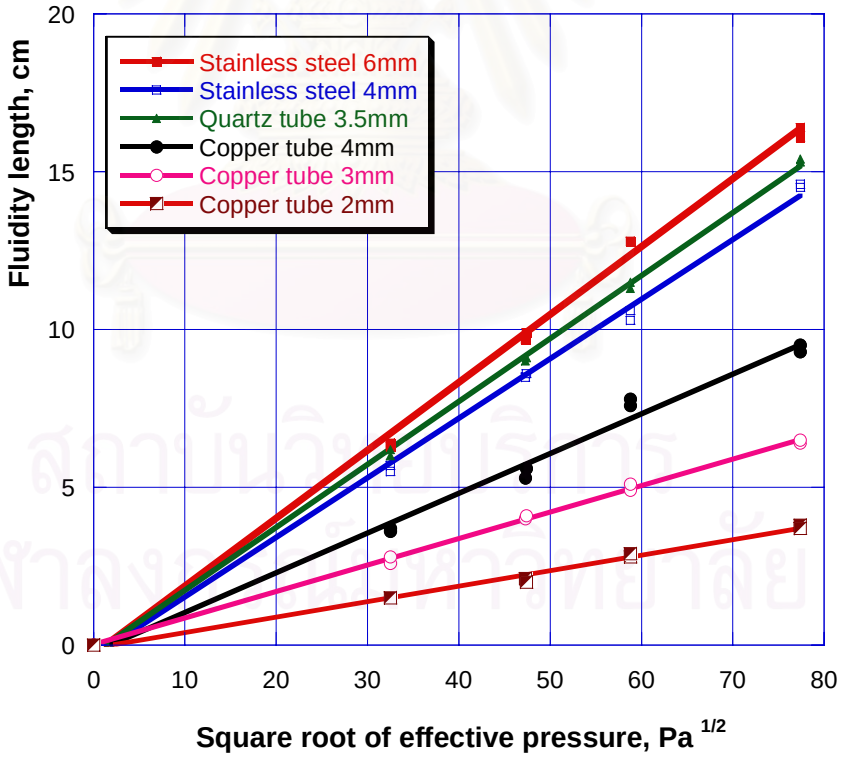

Figure 36. Relationship between fluidity and square root of effective pressure at 973 K (ΔT = 85 K), alloy AC2B, estimate with best fit surface energy σ = 1.2 N/m.

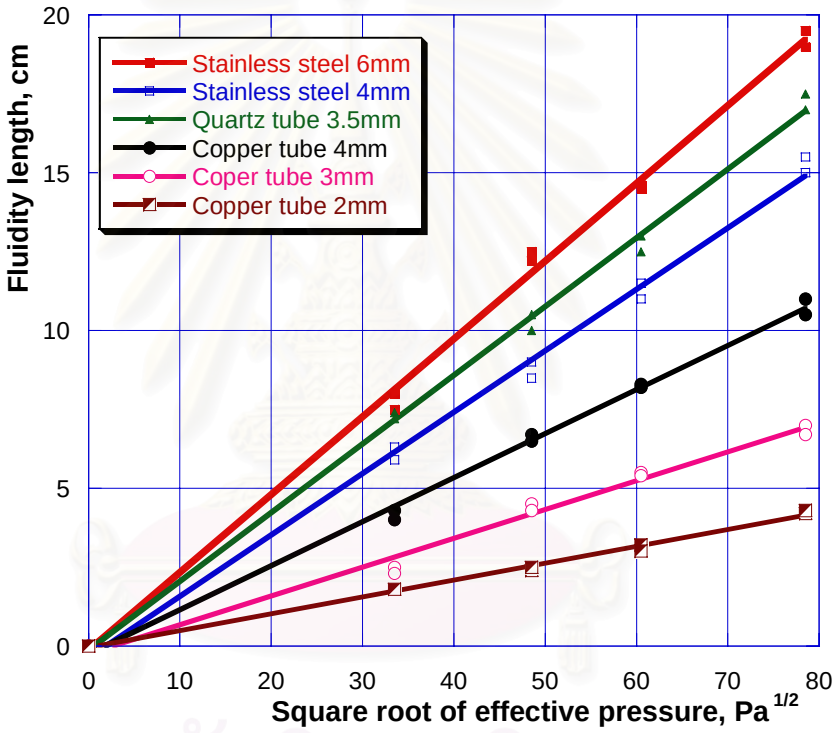

Figure 37. Relationship between fluidity and square root of effective pressure at 973 K (ΔT = 85 K), alloy AC4CH, estimate with best fit surface energy σ = 1.15 N/m

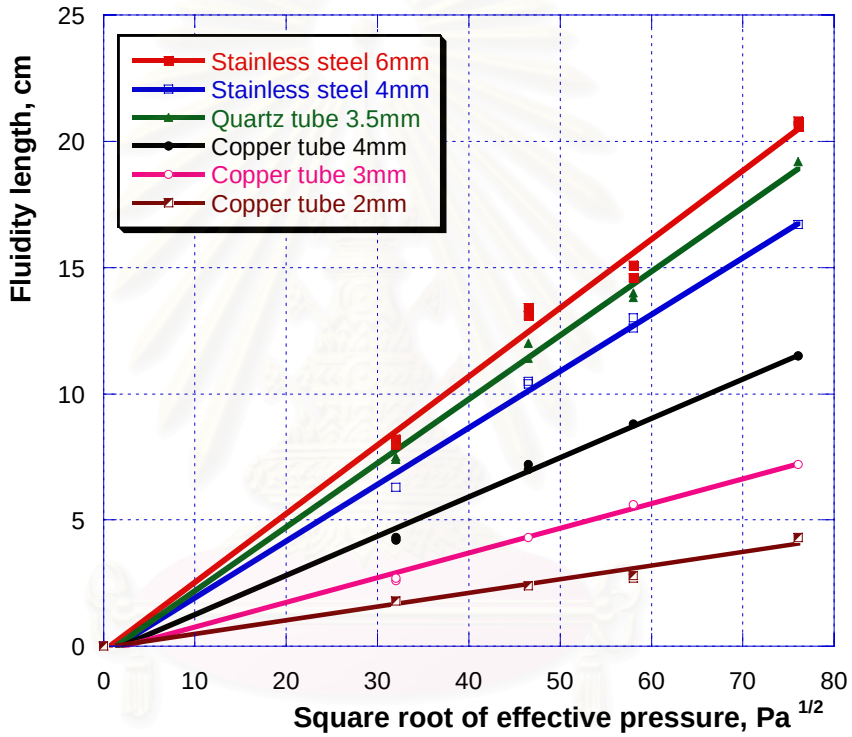

Figure 38. Relationship between fluidity and square root of effective pressure at 973 K (ΔT = 110 K), alloy AC4B, surface energy σ = 1 N/m.

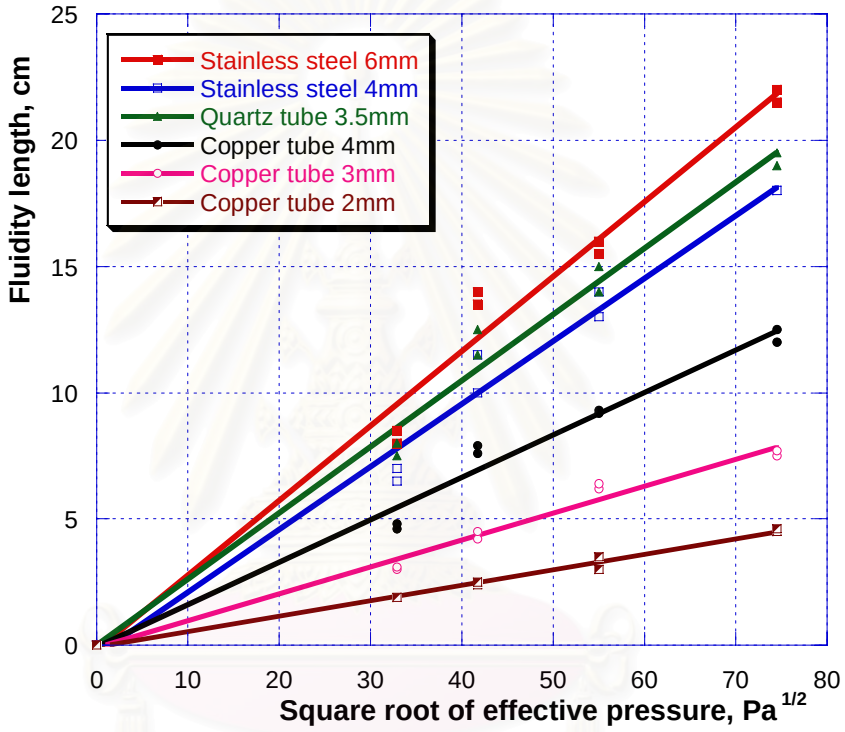

Figure 39. Relationship between fluidity and square root of effective pressure at 973 (ΔT = 115 K), alloy ADC12, surface energy σ = 0.9 N/m.

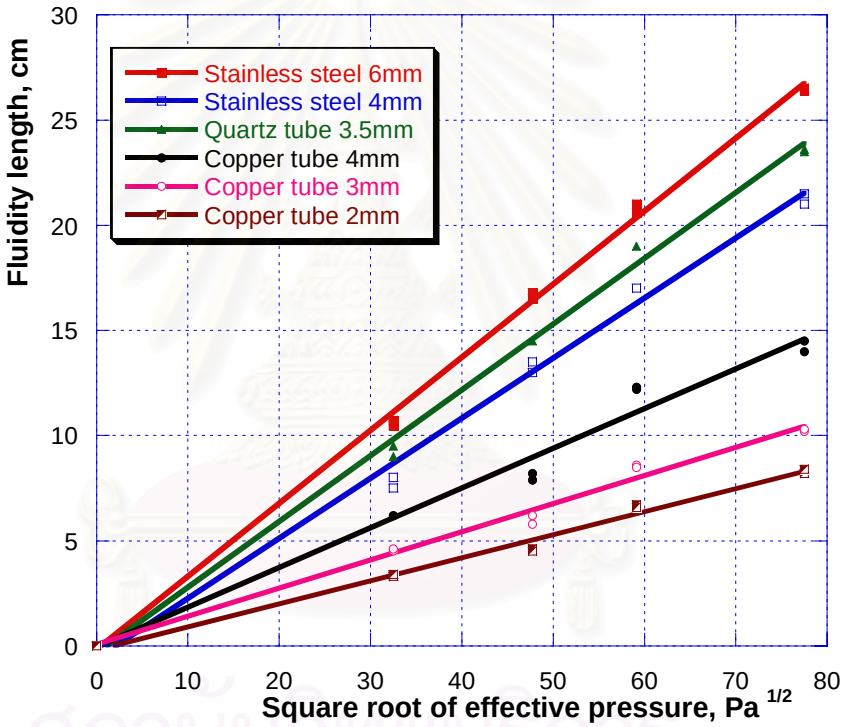

Figure 40. Relationship between fluidity and square root of effective pressure at 973 K (ΔT = 60 K), alloy ADC14, surface energy

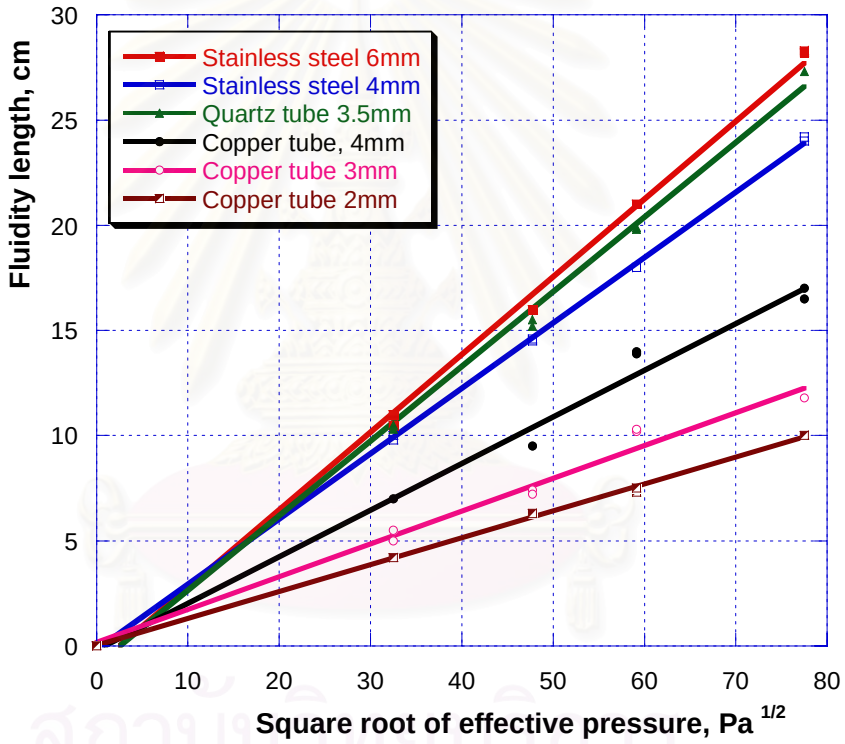

Figure 41. Relationship between fluidity and square root of effective pressure at 1073 K (ΔT = 60 K), alloy AC9A, surface energy

From calculation, value of surface energy is obtained. It is found that surface energy was decreases by increasing silicon content. Relationship of surface energy and alloys is shown in figure 44

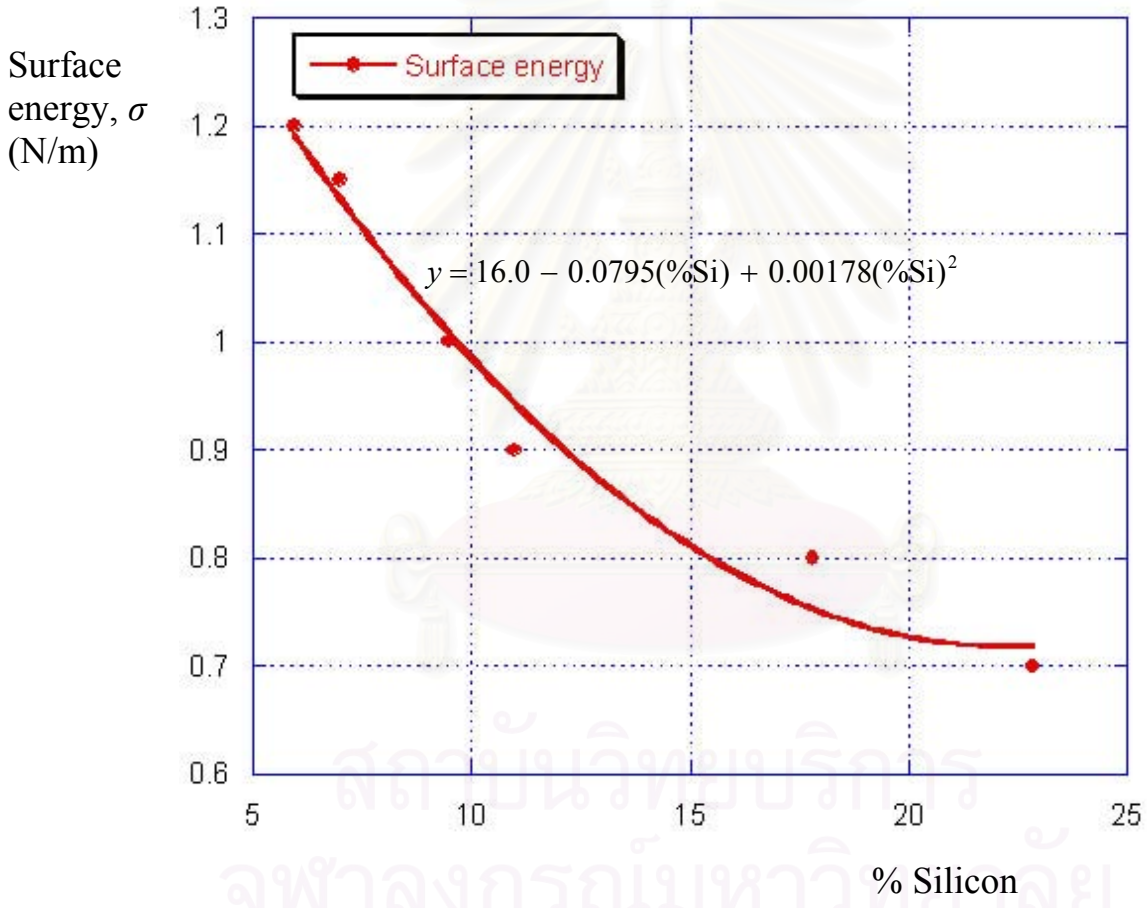

Figure 42. Relationship between silicon content and surface energy

Figure 20 shows the fluidity under applied suction pressure ΔP_a=6.67 kPa and $\Delta T = 90$ K, of aluminum alloys into different mold materials of which diameter is almost same; 4 mm for copper and stainless steel tubes and 3.5 mm for quartz tube. It increased significantly with hypereutectic alloys. Ranking order of fluidity of each mold material is shown as the same order as different materials.

5.2 Solidification of aluminum alloys in the fluidity test

As discussed earlier, metal flow continues through inter-grain paths at the latter stages of solidification, before flow stops. At these stages, the shape and size of paths play an important role in the microstructure. In hypoeutectic aluminum silicon alloys, the proeutectic phases appear as α dendrites and the paths are narrow; they interfere effectively with the flowing metal (flow is captured completely) figure 5. In hypereutectic Al-Si alloys, the proeutectic phases are primary Si particle and the paths are not tortuous. Therefore, when the metal flow almost ceases and most primary particles remain, some flow can continue without being captured by proeutectic silicon particle. In this situation, a proeutectic Si-free zone develops.

Aluminum alloy fluidity test castings were investigated metallographically. Generally, these microstructures agree with Fleming theory, in that fine, random, equiaxed grains are found at the tip. And well developed columnar dendrites are found at the beginning of the fluidity test channel figure 4 and figure 20. Smaller grains exist at the tip of the fluidity test channel where there is less time and space to develop

a columnar dendrite structure, while larger grains exist at the beginning of the test casting channel.

All fluidity test castings show microstructures that have only few proeutectic Si particles at the tip. In hypoeutectic, proeutectic phases appear as alpha dendrites, and hypereutectic Al-Si alloys, they are primary Si particles. Furthermore, dimples are observed at the tip of these casting. This implies that the metal flow does not cease by the solidification at the tip.

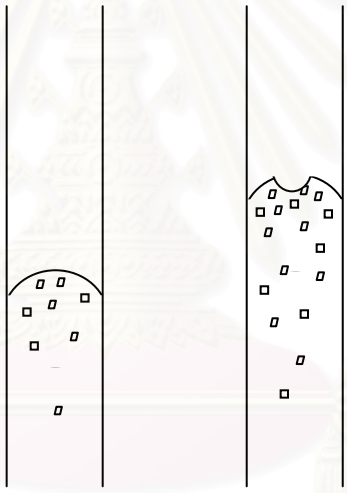

Figure 43. Solidification of aluminum alloys in channel of fluidity test mold.

In the case of alloys without superheat, the nucleation of fine grains at the tip is immediate. However, if the metal has superheat, nucleation is delay and result in an increased fluidity length; as a result, superheat is the principle factor that increased fluidity.

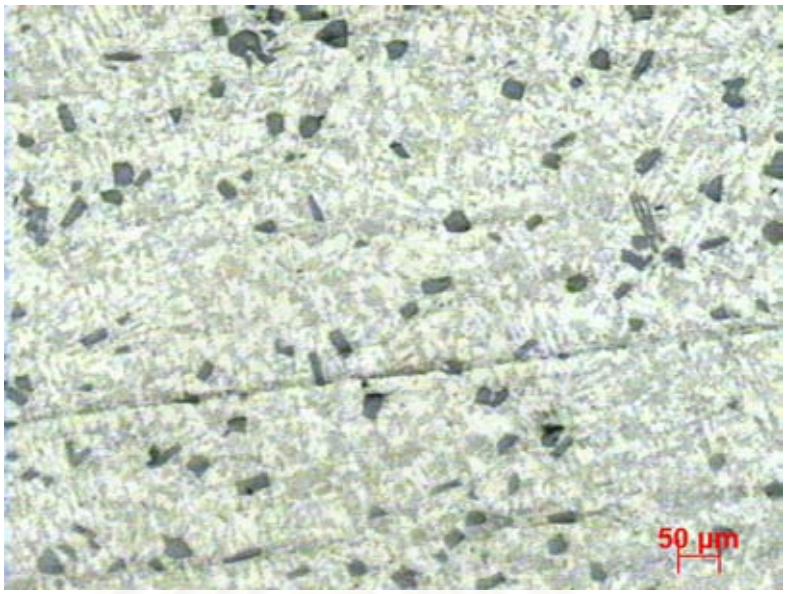

Figure 44. Microstructure of alloy ADC14 at tip test channel

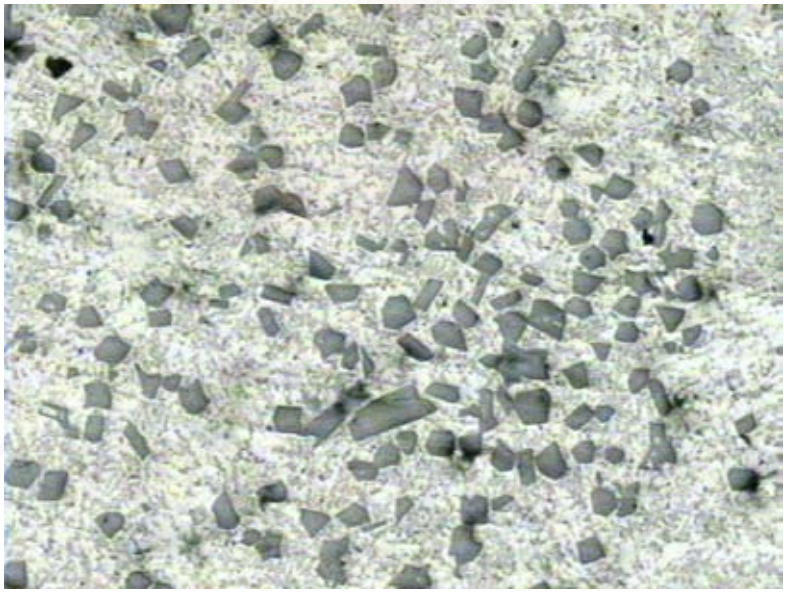

Figure 45. Microstructure of alloy ADC14 at middle test channel

5.3 High vacuum and positions

Nowadays, high vacuum die casting becoming popular using 5 kPa absolute pressures, conversely to suction pressure is 95 kPa. In this research, high vacuum is done with two cases of positions: horizontal and vertical. These two cases can be used to compare the effect of gravity into fluidity length. From this finding, apply them into real case and to simulation also. The difference between two cases can calculate and state that effect of gravity hold 6% of applied suction pressure.

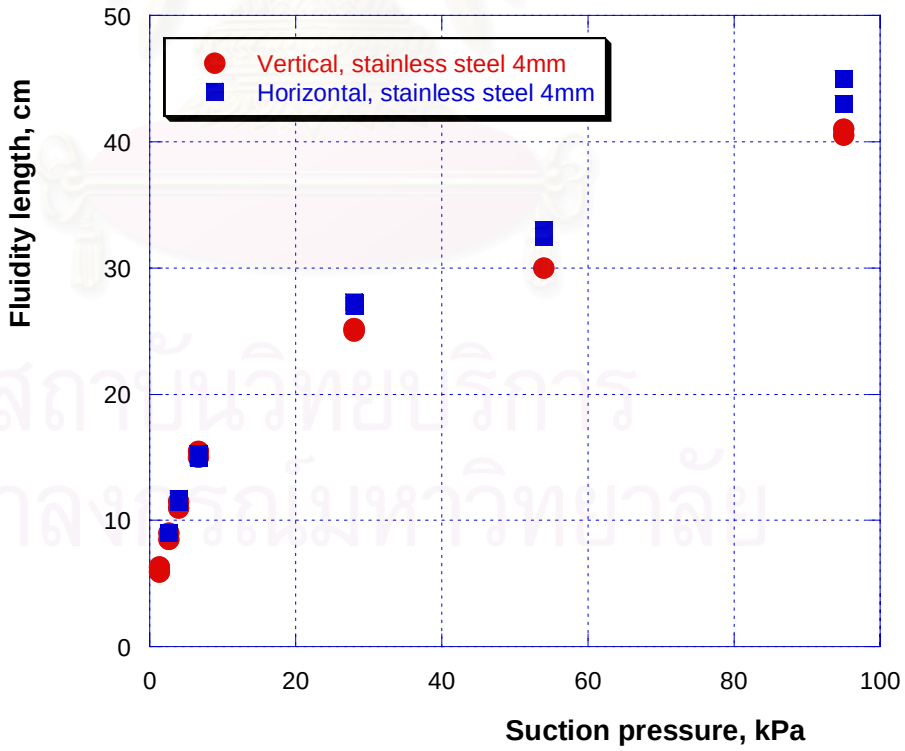

Figure 46. Fluidity of alloy AC4CH, high vacuum and positions.

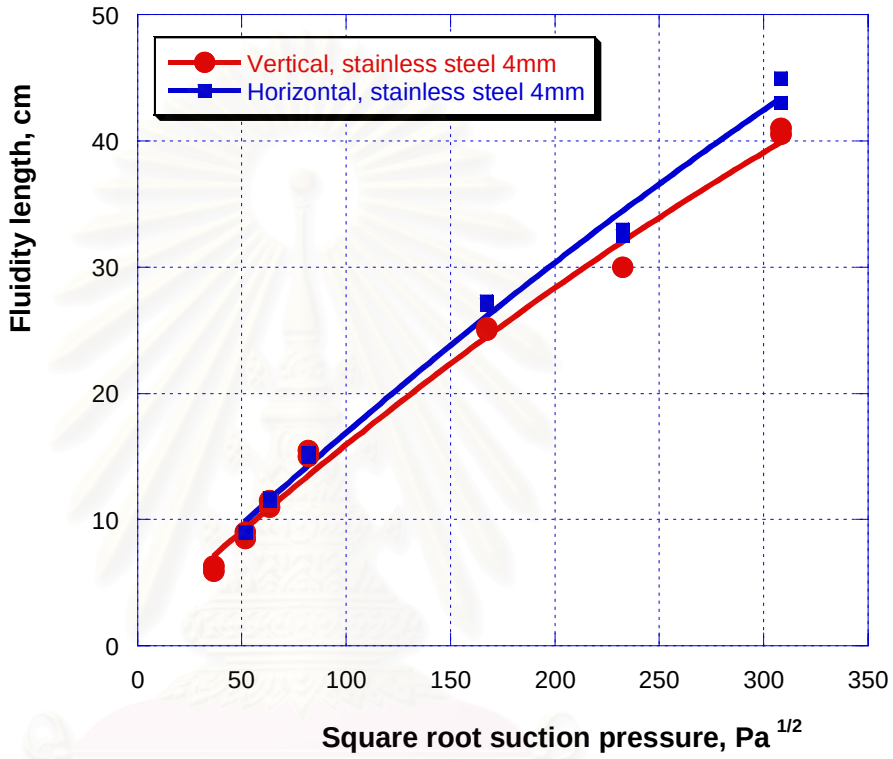

Figure 47. Estimate effect of gravity

From figure 47, we observe and see that square root of suction pressure (308 $Pa^{1/2}$) is 4 time greater than the case low suction pressure (82 $Pa^{1/2}$) but the fluidity is not 4 times longer, only about 2.5 time longer. This is because of solidification mechanism occurrence. According to Flemings, flow ceases at the leading tip of the flowing stream where it forms columnar dendrites. The dendrite arms expose and fracture forming equiaxed grains.

Chapter 6

Conclusions

Fluidity of aluminum alloys AC2B, AC4CH, AC4B, AC9A, ADC12 and ADC14 was investigated. Microstructure of fluidity test channel was observed. The following conclusions have been drawn from the experimental results and discussions:

1. Fluidity of aluminum alloys is found linear with square root of applied suction pressure. Relationship between fluidity and diameter of mold material, degree of superheat are also linear.

2. Fluidity results are not the same with different mold materials because heat transfer coefficient *h* effects to the interface between mold and casting.

3. By estimating the relationship of fluidity and effective pressure, considering the effectiveness of surface energy, it is found that surface energy decreases by increasing silicon content. Fluidity is found as a function of silicon content. Therefore surface energy will decreases by increasing silicon content and fluidity.

4. The increasing fluidity of aluminum alloys is obtained in the hypereutectic region.

5. Minimum applied suction pressure required to suck the liquid is calculated in the range from 40 to 200 Pa, depending on type of alloys.

6. Different alloy solidification obtained different microstructures with intermetallic phases match Flemings theory.

Future works

- Estimate “fraction of solid criteria” for each alloy
- Temperature and filling time measurements of the flow in channel
- Flow simulation

References

1. Merton C. Fleming: *Solidification Processing*, 1st Edition, McGraw-Hill, Inc (1974).
2. Peter Beeley: *Foundry Technology*, 2nd Edition, Butterworth-Heinemann (2001).
3. M. Tiryakioglu, D.R. Askeland, C.W. Ramsay: "*Fluidity of 319 and 356: An Experiment Design Approach*," Trans. Am. Fndrym. Soc., Vol 102 pp17-25(1994).
4. Metals Handbook, vol 2, 10th Edition, ASM International Metals Park (1990).
5. Metals Handbook, vol 15, 10th Edition, ASM International Metals Park (1990).
6. John E. Gruzleski, Bernard M. Closset: *The Treatment of Liquid Aluminum-Silicon Alloys*, 1st Edition, The American Foundry's Society, Inc (2000).
7. Donna L. Zalensas: *Aluminum Casting Technology*, 2nd Edition, The American Foundry's Society, Inc (1997).
8. Q. Kubachuski, C. B. Alcock, P. J. Spencer: *Materials thermo-chemistry*, 6th Edition, Pergamon Press.
9. S. Gowvi and F.H Sanmuel: *Effect of alloying element on the solidification Characteristics and microstructure of Al-Si-Cu-Mg-Fe 380 alloy*. Met Trans Vol 25A Feb 1994(page 437)
10. A.K Dahle, P.A Tondel, C.J Paradises and L. Arnberg: *Effect of Grain refinement on the fluidity of two commercial Al-Si alloys*. Met Trans Vol 27A Aug, 1996
11. J.X Dong, P.A Karnezis, G Durant, and B Cantor: *The effect of Sr and Fe addition on the microstructure and mechanical properties of a direct squeeze cast Al-7Si-0.3Mg*. Met Trans Vol 30A May 1999.
12. J. M. Kim, C.R. Loper, Jr: *Effect of solidification Mechanism on fluidity of Al-Si casting alloys*. AFS Transaction Vol 103, pp 521-529 (1995).
13. D.Emadi, J. E. Gruzleski, and J.M Toguri : *The effect of Na and Sr modification on surface tension and volumetric shrinkage of A356 alloy and their influence on porosity formation.* Met Trans Vol 24B Dec, 1993.

14. Y.W. Lee, E. Chang and C. F Chieu: *Modeling of feeding behavior of solidifying Al-7Si-0.3Mg alloy plate casting.* Met Trans vol 21B Aug 1990.
15. A.K.Jena, A.K Gupta, and C. Chaturuedi: *Effect of silicon addition on the first stage of precipitation in the Al-1.5pct Cu-0.75pct Mg alloy.* Met Trans Vol 24A Oct, 1993.
16. D.L Zhang; B. Canton: *Heterogeneous Nucleation of Solidification of Silicon by Solid aluminum in hypoeutectic Aluminum Silicon alloy*. Met Trans Vol 24A May, 1993.
17. F. Michel, P.R Louchez, and F.H. Samuel: *Effect Heat Transfer Coefficient During Solidification of Al-Si alloys*. AFS Transaction Vol 103, pp 275-284 (1995).
18. Wanqi Jie, Zhongwei Chen, W. Reif and K. Muller: *Superheat Treatment of Al-7Si-0.55Mg and Its Influences on the Solidification Structures and the Mechanical Properties.* Met Trans Vol 34A Mar, 2003.
19. P. Suwanpinij, U. Kitkamthorn, I. Dewwanit and T. Umeda *Solidification Characteristic of A356, A380, A390 Aluminum Alloys and the Influence from Copper and Iron*. 7th Asian Foundry Congress, Taiwan 2001.
20. George E. Totten, D. Scott MacKenzai: *Handbook of Aluminum*, 1st Edition, Marcel Dekker, Inc (2003).
21. OKANE Toshimitsu, MARU Naoki, AKASHI Takafumi, NAKAJIMA Ichiro, WADA Manabu and AKIMOTO Jun: *Fluidity of Copper alloy and Aluminum Alloy*. 8th Asian Foundry Congress, Bangkok 2003.
22. Sadato Hiratsuka, Eisuke Niyama, Tatsuya Funakubo and Koichi Anzai: *Effects of Mold Coating and Mold Atmosphere on the Fluidity of an Aluminum Alloy*. Transactions of the Japan Foundryman's Society. Vol. 13. November, 1994.

Appendices

APPENDIX 1

The rate of heat flow across the mold-metal interface

Follow Fleming; consider first the problem of unidirectional heat flow and the solution conform to equation:

$$\frac{\partial T}{\partial t} = \alpha_m \frac{\partial^2 T}{\partial x^2} \qquad (1)$$

α_m is thermal diffusivity of mold, cm^2/s. $\alpha = \frac{K}{\rho C_P}$, K is thermal conductivity, ρ is density and C_p is specific heat.

Boundary condition:

$$x = 0 \qquad T = T_M \qquad (2)$$

$$x \to \infty \quad T \to T_0 \qquad (3)$$

Initial condition:

$$t = 0 \qquad T = T_0 \qquad (4)$$

Assumed that T is a function of $\frac{x^2}{t}$, that mean $T = f\left(x^2/t\right)$. So, a new variable is defined as:

$$\eta = x/\left(2\sqrt{K.t}\right) \qquad (5)$$

so, $$\frac{\partial \eta}{\partial x} = \frac{1}{2\sqrt{\alpha t}} = \frac{\eta}{x}, \quad \frac{\partial^2 \eta}{\partial x^2} = -\frac{\eta}{x^2} + \frac{1}{x}\frac{\partial \eta}{\partial x} = -\frac{\eta}{x^2} + \frac{\eta}{x^2} = 0$$

and $$\frac{\partial \eta}{\partial t} = -\frac{x}{4\sqrt{K}t^{3/2}} = -\frac{\eta}{2t}$$

$$\frac{\partial^2 T}{\partial x^2} = \frac{\partial}{\partial x}\left(\frac{\partial \eta}{\partial x}\frac{dT}{d\eta}\right) = \frac{\partial^2 \eta}{\partial x^2}\frac{dT}{d\eta} + \frac{\partial \eta}{\partial x}\frac{\partial}{\partial x}\left(\frac{dT}{d\eta}\right) = \frac{\partial \eta}{\partial x}\frac{\partial \eta}{\partial x}\frac{d}{d\eta}\left(\frac{dT}{d\eta}\right) = \frac{\eta^2}{x^2}\frac{d^2 T}{d\eta^2}$$

$$\frac{\partial T}{\partial t} = \frac{\partial \eta}{\partial t}\frac{dT}{\partial \eta} = -\frac{1}{2}\frac{\eta}{t}\frac{dT}{d\eta}$$

Substitute to equation (1), reduce to:

$$-\frac{1}{2}\frac{\eta}{t}\frac{dT}{d\eta} = K\frac{\eta^2}{x^2}\frac{dT^2}{d\eta^2}$$

$$\frac{dT^2}{d\eta^2} + \frac{1}{2}\frac{x^2}{Kt}\frac{1}{\eta}\frac{dT}{d\eta} = 0$$

from (5) $\eta^2 = \frac{x^2}{4\alpha t}$ so we obtain

$$\frac{d^2T}{d\eta^2} + 2\eta\frac{dT}{d\eta} = 0 \tag{6}$$

if we defined $\frac{dT}{d\eta} = S$, equation (6) become:

$$\begin{aligned} &\frac{dS}{d\eta} + 2\eta S = 0 \\ &\frac{dS}{S} = -2\eta d\eta \\ &\ln S = -\eta^2 \\ &S = C_1 \exp\left(-\eta^2\right) \end{aligned} \tag{7}$$

Because of the definition: $\frac{dT}{d\eta} = S$, so we obtain:

$$\begin{aligned} &\frac{dT}{d\eta} = C_1 \exp\left(-\eta^2\right) \\ &T = C_1 \int_0^{\eta} \exp\left(-z^2\right) dz + C_2 \end{aligned} \tag{8}$$

Boundary conditions reduce to:

$$\eta = 0 \qquad T = T_M \tag{9}$$

$$\eta \to \infty \qquad T \to T_0 \tag{10}$$

from (9), we obtain $C_2 = T_M$

from (10),

$$\begin{aligned} &T_0 = C_1 \int_0^{\infty} \exp\left(-z^2\right) dz + T_M \\ &C_1 = \frac{T_C - T_0}{\int e^{-x^2} dx} = \frac{2}{\sqrt{\pi}}\left(T_M - T_0\right) \end{aligned} \tag{11}$$

Substitute (11) to (8), we get temperature profile;

$$T = \frac{2}{\sqrt{\pi}}\left(T_C - T_0\right) \int_0^{x/2\sqrt{Kt}} e^{-z^2} dz + T_C$$

or $$\frac{T - T_C}{T_0 - T_C} \frac{2}{\sqrt{\pi}} \int_0^{x/2\sqrt{Kt}} e^{-z^2} dz = erf\left(x/2\sqrt{Kt} \right)$$

The rate heat flow into the mold at the mold-metal interface is given by:

$$\left(\frac{q}{A} \right)_{x=0} = K_m \left(\frac{\partial T}{\partial x} \right)_{x=0}$$

from temperature profile:

$$T = \frac{2}{\sqrt{\pi}} (T_M - T_0) \int_0^{x/2\sqrt{\alpha t}} e^{-z^2} dz + T_M$$

$$\frac{\partial T}{\partial x} = \frac{2}{\sqrt{\pi}} (T_0 - T_M) \frac{1}{2\sqrt{\alpha t}} e^{-x^2/4\alpha t}$$

$$\left(\frac{q}{A} \right)_{x=0} = \frac{2}{\sqrt{\pi}} (T_0 - T_M) \frac{K}{2\sqrt{\alpha t}} = -(T_M - T_0) \sqrt{\frac{K\rho C_p}{\pi t}}$$

note that:

$$\frac{K}{\sqrt{\alpha}} = \frac{K}{\sqrt{\frac{K}{\rho C_p}}} = \sqrt{K\rho C_p}$$

The rate of heat flow across the mold-metal interface seen to be:

$$\left(\frac{q}{A} \right)_{x=0} = -\sqrt{\frac{K_m \rho_m c_m}{\pi t}} (T_M - T_0)$$

here, heat diffusivity $\alpha = \frac{K}{\rho C_p}$, K is thermal conductivity, ρ is density and C_p is specific heat.

APPENDIX 2

Modulus

Follow Fleming; consider first the problem of unidirectional heat flow and the solution conform to equation:

$$\frac{\partial T}{\partial t} = \alpha_m \frac{\partial^2 T}{\partial x^2}$$

α_m is thermal diffusivity of mold, cm^2/s.

The rate heat flow into the mold at the mold-metal interface is given by:

$$\left(\frac{q}{A}\right)_{x=0} = K_m \left(\frac{\partial T}{\partial x}\right)_{x=0}$$

from temperature profile:

$$T = \frac{2}{\sqrt{\pi}}(T_M - T_0) \int_0^{x/2\sqrt{\alpha t}} e^{-z^2} dz + T_M$$

$$\frac{\partial T}{\partial x} = \frac{2}{\sqrt{\pi}}(T_0 - T_M)\frac{1}{2\sqrt{\alpha t}} e^{-x^2/4\alpha t}$$

$$\left(\frac{q}{A}\right)_{x=0} = \frac{2}{\sqrt{\pi}}(T_0 - T_M)\frac{K}{2\sqrt{\alpha t}} = -(T_M - T_0)\sqrt{\frac{K\rho C_p}{\pi t}}$$

The rate of heat flow across the mold-metal interface seen to be:

$$\left(\frac{q}{A}\right)_{x=0} = -\sqrt{\frac{K_m \rho_m c_m}{\pi t}}(T_M - T_0)$$

here, heat diffusivity $\alpha = \frac{K}{\rho C_p}$, K is thermal conductivity, ρ is density and C_p is specific heat.

$$\frac{K}{\sqrt{\alpha}} = \frac{K}{\sqrt{\frac{K}{\rho C_p}}} = \sqrt{K\rho C_p}$$

The heat entering the mould comes only from heat of fusion of the solidifying metal:

$$\left(\frac{q}{A}\right)_{x=0} = -\rho_s H \frac{\partial S}{\partial t}$$

S is thickness of solidified.

$$S = \frac{2}{\sqrt{\pi}}\left(\frac{T_M - T_0}{\rho_s H}\right)\sqrt{K_m \rho_m c_m}\,\sqrt{t}$$

Metal mold

For simple shape, we assume to replace S with V_s/A where V_s is the volume solidified at a time t, and A is the area of the metal mould interface (i.e. the cooling area of the casting) and when $t = t_f$ where t_f is the total freezing time of a casting of volume V we have:

$$\frac{V}{A} = \frac{2}{\sqrt{\pi}}\left(\frac{T_M - T_0}{\rho_s H}\right)\sqrt{K_m \rho_m c_m}\,\sqrt{t_f}$$

and so: $t_f = C\left(\frac{V}{A}\right)^2$ where C is constant for given metal and mould conditions. This is **Chvorinov rule.**

Chvorinov rule stated that: total time of solidification time is proportional to the square of the volume-to-area of the casting. The origin experiment of Chvorinov confirm on steel casting of different sizes and shapes, varying from 10mm thickness to 65 ton casting.

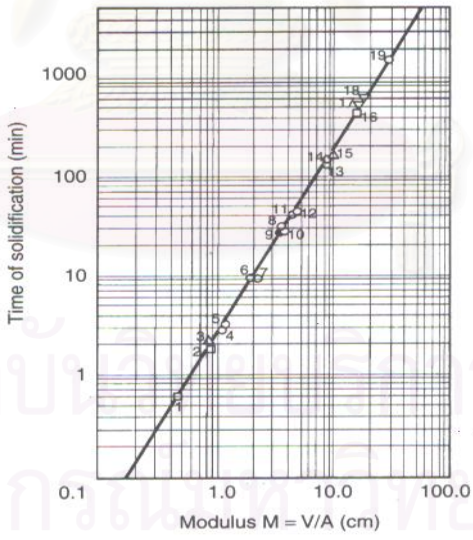

Figure1: Relationship between shape and solidification time for steel casting.

One of the most importances of Chvorinov rule is apply in riser design. When design a riser, the shape, sizes and positions of the riser must be calculated. The sizes and shapes of riser satisfy two requirements. It must be solidified slowly to fed liquid for casting and

the head must be has enough capacity to supply volume of liquid to compensate.

It means that referred to freezing time and volume riser capacity, respectively. In order for riser to cool slower than the main cast, we desired total freezing time must be greater than that of the main casting. The modulus of the riser (M_r) equals 1.2 times the modulus of the casting (M_c). The extra 20% given by this is safety a factor to allow for error and difficulties in calculating the moduli. As we known, modulus is defined as solidifying volume divided by the surface area of the casting. It is emphasized that only those surface lose heat. When modulus increases, solidification time is increase. Therefore modulus is a useful means of predicting solidification time.

The volume of metal to compensate for shrinkage is not so big, normally less than 7%. It is possible to get this condition and in the case of thin plate, the freezing of the casting is accelerated by heavy of chilling or by very low *V/A* ratio.

We see that, freezing time of any solidifying body is controlled by its volume/cooling surface area, known as its modulus, *m*. Here shows some simple shapes:

1. In case of spherical: D is diameter

$$V = \frac{4}{3}\pi.r^3 = \frac{4}{3}\pi\left(\frac{D}{2}\right)^3 = \frac{\pi.D^3}{6}$$

$$A = \pi D^2$$

so, $$m = \frac{V}{A} = \frac{D}{6} = 0.167D$$

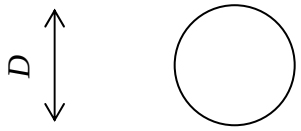

2. In case of cubic

$$V = D^3,\ A = 6D^2,$$

$$m = \frac{V}{A} = \frac{D}{6} = 0.167D$$

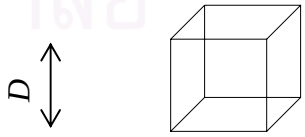

3. In case of infinite plate:

$$V = a.b.D$$

$$A = 2.a.b$$

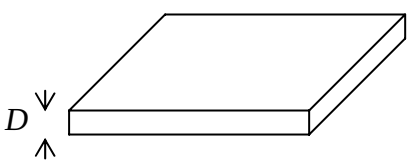

$$m = \frac{V}{A} = \frac{D}{2} = 0.5D$$

4. In case of rod/infinite cylindrical

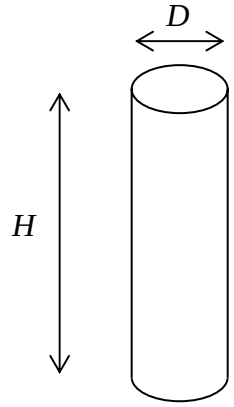

$$V = \frac{\pi}{4} D^2 H$$
$$A = \pi.D.H$$
$$m = \frac{V}{A} = \frac{D}{4} = 0.25D$$

In experiment procedure, it has been done with the tube (we consider that is similar with the case of rod) D = 5mm. It mean that, m = 1.25mm. From this experiment, we can apply in case of plate with m = 2.5mm. In all experiments, we need to run in the same modulus in order to compare and apply in practice easily.

APPENDIX 3

Bernoulli's Equation

The most useful relation in engineering hydraulics is really three

---

Daniel Bernoulli disclosed the equation used most frequently in engineering hydraulics in 1738. This equation relates the pressure, velocity and height in the steady motion of an ideal fluid. The usual form is $v^2/2 + p/\rho + gz = \text{constant}$, where v is the velocity at a point, p the pressure, ρ the density, g the acceleration of gravity, and z the height above an arbitrary reference level. Students apply the equation without much thought, sometimes inappropriately, and have no clear idea of the conditions under which it is applicable. It appears on every general engineering examination, since it is easy to trap the unwary. Actually, it is not one relation, but three, all apparently of the same form, but applying in different situations. The three forms will be explained in this paper.

$$\frac{\partial \mathbf{v}}{\partial t} + \mathbf{v}\cdot\nabla\mathbf{v} = \mathbf{F} - \frac{1}{\rho}\nabla p \quad \text{Euler's equation}$$

$\mathbf{v} = -\nabla\phi$ so $\nabla \times \mathbf{v} = 0$ irrotational

$\mathbf{F} = -\nabla\Omega$ conservative

$\rho = \text{const. or } f(p)$ incompressible

$$\frac{\partial}{\partial t}\left(-\nabla\phi\right) + \nabla\phi\cdot\nabla\nabla\phi = -\nabla\Omega - \frac{1}{\rho}\nabla p$$

$$\nabla\left[-\frac{\partial\phi}{\partial t} + \frac{v^2}{2} + \Omega + \frac{p}{\rho}\right] = 0$$

$$-\frac{\partial\phi}{\partial t} + \frac{v^2}{2} + \Omega + \frac{p}{\rho} = C$$

$$\frac{v^2}{2} + \Omega + \frac{p}{\rho} = C \quad \text{Bernoulli's equation}$$

Bernoulli's Equation

The most powerful form of Bernoulli's Equation is derived from the Eulerian equations of motion under rather severe restrictions. First, the velocity must be derivable from a velocity potential. Second, external forces must be conservative--that is, derivable from a potential. Thirdly, the density must either be constant or a function of the pressure alone. In particular, thermal differences, such as occur in natural convection, are excluded. Here, we will assume the fluid is incompressible for simplicity, but it is possible to write a similar equation for compressible fluids. Vector notation is used in the Figure to show that the gradient of a certain expression becomes zero under these assumptions, and Bernoulli's Equation follows on integration and the introduction of the condition of steady motion. It is probably clearer to do the derivation with rectangular components, and to see how the condition curl **v** = 0 is used. The gradient of a dot product is a rather complicated thing, incidentally.

This form of Bernoulli's Equation applies to steady irrotational flow, and the constant is really a constant throughout the volume of irrotational flow. Nothing is said about streamlines.

The second form of Bernoulli's Equation arises from the fact that in steady flow the particles of fluid move along fixed streamlines, as on rails, and are accelerated and decelerated by the forces acting tangent to the sreamlines. Under the same assumptions for the external forces and the density, but without demanding irrotational flow, we have for an equation of motion $dv/dt = v(dv/ds) = -d\Omega/ds - (1/\rho)dp/ds$, where s is distance along the streamline. This integrates immediately to $v^2/2 + \Omega + p/\rho = c$. In this case, the constant c is for the streamline considered alone; nothing can be said about other streamlines. This form of Bernoulli's Equation is more generally applicable, but less powerful than the preceding one. It is the form most often applicable to typical engineering problems. The derivation is easy and straightforward, clearly showing the hypotheses, and also that the motion is assumed frictionless.

The third form of Bernoulli's Equation is derived from the conservation of energy. Bernoulli himself took an equivalent approach, although the concept of energy was not well-developed in his time. Energy balance is a favoured method of approach in engineering, and this is the usual derivation of Bernoulli's Equation in elementary work. By the use of energy concepts, the equation can be extended usefully to compressible fluids and thermodynamic processes. In the Figure, an element of fluid is transferred from one point to another in a tube with rigid boundaries. The equation of continuity for an incompressible fluid shows that the same volume of fluid Q disappears at one point and reappears at another. The imaginary pistons move with the speed of the fluid. Capital letters are used for quantities at one point, small letters for the same quantities at the second point. The energies per unit volume, made up of kinetic, potential, and pressure terms are equated. The pressure terms can also be handled as doing work on the element of fluid, which is equivalent. The virtue of this derivation is that can be extended in various directions to give important results, and that it is easily believed by students. The rigid tube can be replaced by a surface generated by streamlines, which can be shrunk down to the

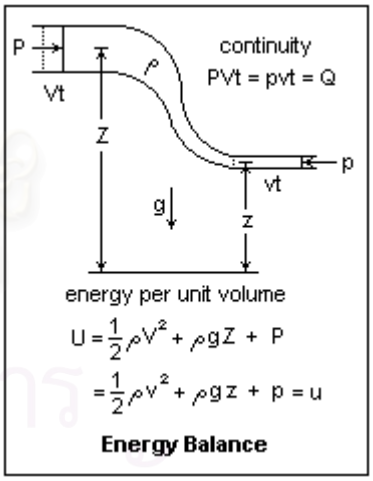

Energy Balance

neighbourhood of a single streamline, which is just the second form of Bernoulli's Equation, but here derived, by energy instead of by dynamics.

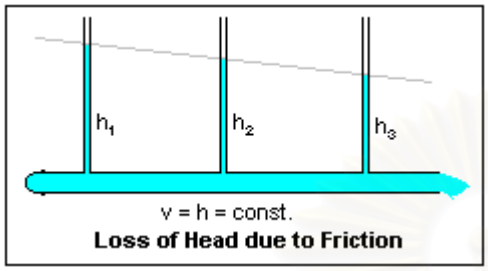

The energy balance method can be extended to allow for friction, by assuming a loss of energy, or 'head' when expressed in terms of potential energy, between the two sections. The height of liquid in each of the vertical tubes is p/ρ, where p is the gauge pressure. Streamlines do not run up the tubes from inside the main tubes, so they measure just pressure, not total energy. Loss of energy is shown by the decrease in the heights, along the *hydraulic gradient*, which corresponds to a loss of energy in the flow. The velocity is constant since we have assumed a uniform pipe, so the pressure gradient is the same as the hydraulic gradient. The loss of head per unit length is often assumed proportional to the square of the velocity, for example as $fv^2/2g$, where f is the *friction factor*, since the flow is usually turbulent.

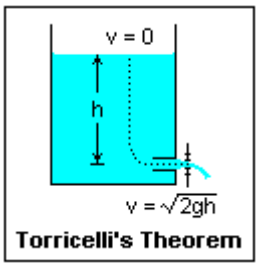

As an example of the use of Bernoulli's Equation, the classic problem of the velocity of efflux through a hole in the side of a tank. We imagine a streamline beginning at the free surface, where the velocity is zero, and extending into the jet a distance h below (dotted in the Figure). The pressures at the two points are the same, atmospheric. From the second (or third) form, we get $gh = v^2/2$, or $v = (2gh)^{1/2}$, which is called Torricelli's Theorem. This does not give us the rate of efflux, however, because the area of the jet is smaller than the area of the hole in the tank. The smallest jet area occurs when the sides of the jet are parallel, which is just the point we used in applying Bernoulli. This point is called the *vena contracta*, and has an area half, or somewhat more, of the area of the hole. For a circular hole in a thin wall, the fraction is 0.62, and if the hole has a tube of the same diameter extending into the tank (a Borda's mouthpiece, as shown in the Figure) the fraction is practically 0.50.

The reason for the fraction 1/2 can be seen by a nice application of the conservation of momentum. The momentum carried away by the fluid moving through the vena contracta is $v^2\rho S'$, where S' is the area of the vena contracta, and the reaction on the container is equal and opposite.

But we can also find the force on the container from the pressure distribution over the walls. The pressure on the hole of area S is zero, but that on an equal area on the other side of the tank is ρghS. This must also be the reaction on the tank due to the escaping fluid. Bernoulli tells us that $v^2 = 2gh$, so equating these two forces, we have $\rho ghS = 2gh\rho S'$, or $S' = S/2$. Borda's mouthpiece makes the pressure the static value right up to the edge of the hole; with a plane hole, the pressure is reduced, so $S' > S/2$ in this case.

Suppose that you have a given amount of liquid Q that you wish to discharge from a cylindrical tank through a hole of area A at the bottom of the tank. Is there an optimum shape of tank that will do this in a minimum time? How long would it take to empty such a tank anyway? The behaviour of the free jet after leaving the aperture is also a subject of interest.

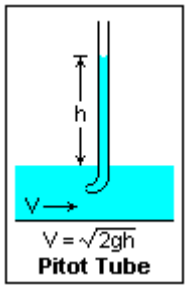

The Pitot tube measures flow velocity by converting the velocity to pressure at the *stagnation point* at a small entry to the manometer tube pointing into the flow. This works for air as well, with an appropriate pressure gauge, reminding us that air behaves as nearly incompressible at speeds well below the speed of sound. Another important example is the Venturi flow meter, where the fluid is made to pass through passages of different areas. The rate of flow is determined from the difference in pressures (heights of manometers) at the two sections. The difference in velocity is found from continuity, and then the difference in pressure from Bernoulli. The increase in velocity in the throat is accompanied by a decrease in pressure there. If $r = A_1/A_2$, then $v_1 = [2g\Delta h/(r^2 - 1)]^{1/2}$, where the symbols are defined in the Figure.

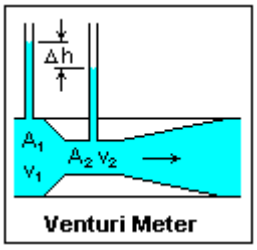

We have now seen the three different theorems that are included under the name of Bernoulli's Equation. All are for steady flow of an incompressible, nonviscous fluid. The first is valid in irrotational flow, the second along a streamline, and the third for an energy-conserving flow in a tube. All look exactly the same when written down. They are capable of being extended to situations different from these by suitable modifications, especially the last one.

Biography

The author was born on October 26, 1978 in Thai Nguyen, a city in the North of Viet Nam. His parents are Tran Van Hao and Tran Thi Hy. He has two sisters, six and three years elder, respectively. He received his Bachelor's Degree in Metallurgical Engineering from Hanoi University of Technology in June, 2001. While a student there, he was a monitor during 5 years of study. Immediately after graduated, he started to work as staff at Department of Materials and Foundry Technology, Hanoi University of Technology.